이학박사학위논문

기억형성에 의한 엔그램 세포 사이의 시냅스 변화에 대한 연구

Studies on synaptic changes among engram cells after memory formation

2019년 2월

서울대학교 대학원

생명과학부

김 지 일

ABSTRACT

Studies on synaptic changes among engram cells after memory formation

Ji-il Kim

School of Biological Sciences

The Graduate School

Seoul National University

The specific sites responsible for memory storage has been focused for a long time. Recent studies demonstrated that memory is encoded in engram cells distributed across the brain. However, the memory substrate at synapse-level within these engram cells remains theoretical while it is generally accepted that synaptic plasticity encodes memory. Because of technical limitations, synapses between engram cells with other synapses has not yet been directly compared. To study engram in synapse-level, I developed dual-eGRASP technique to differentiate the synapses in one dendrite based on its presynaptic neuronal population. By comparing the four possible synapses (engram to engram, engram to non-engram, non-engram to engram, non-engram to non-engram) between CA3 – CA1 connections, I found the increased number and size of spines on CA1 engram cells received input from CA3 engram cells than other synapses. In

addition, electrophysiological experiments revealed the functional enhancement of synapses between engram cells by showing CA3 engram synapses exhibit increased release probability, while CA1 engram synapses exhibit enhanced postsynaptic responses. These results strongly suggest that increased structural and functional connectivity between engram cells across two directly connected brain regions forms the synaptic correlate of memory.

.....

Keywords : Memory, Hippocampus, Engram, Synaptic plasticity

Student Number : 2014-21265

CONTENTS

LIST OF FIGURES

CHAPTER I

INTRODUCTION

BACKGROUND

The question “How and where is memory encoded in our brain?” has been received much attention in the neuroscience field. Over the past few decades, molecular and cellular approaches have shown that genes, proteins, and various molecules play important roles in learning and memory. These achievements could explain the molecular mechanisms of memory encoding. However, although it has been relatively more studied *how* memory is encoded, the physical substrates *where* encoding memory in our brain still remains to be elucidated.

Contextual Fear Conditioning

To study the memory, various behavioral tasks for model animals have been used to mimic the memory encoding processes. Contextual Fear Conditioning (CFC) is one of the most widely used tasks to quantify the memory performance of animals (Fanselow, 2000). In this task, the mouse is given electric shocks after brief exploring a chamber. When the mouse enters to the same chamber later, it will show “freezing” behavior, which is a fear response of rodents, because the mouse could associate the chamber and electric shocks. Thus, the time percentage of freezing behavior during the retrieval test session could be regarded as an indicator of the memory performance (Fig 1).

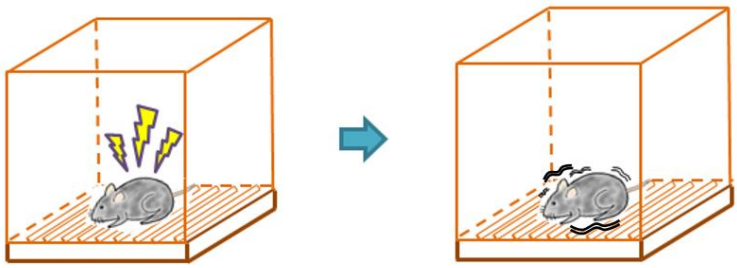

Figure 1. Schematic illustration demonstrating CFC

A mouse was exposed into a context and given electric shocks. After this CFC process, the mouse showed freezing behavior when it exposed to the context again.

Hippocampus

Hippocampus is responsible for the consolidation of episodic memory. Hippocampus consists of several subregions including dentate gyrus (DG), Cornu Ammonis (CA) 3, and CA1. The circuits between subregions inside hippocampus were well defined; DG to CA3 (called mossy fiber pathway) and CA3 to CA1 (called Schaffer collateral pathway). In addition, a hippocampus has linear alignments of cell bodies of neurons. Therefore, we can easily distinguish the cell bodies and dendritic area during recording and imaging. Based on its importance on memory process and relatively simple structure, a hippocampus is appropriate brain region for studying the mechanism of memory encoding.

Hebbian plasticity and Long-term Potentiation (LTP)

To explain how memory is encoded in the synapse-level, Donald O. Hebb proposed a hypothetical mechanism, which is often paraphrased as “Fire together, wire together” (Hebb, 1949). This Hebbian plasticity implies that a strengthening of synapses between co-activated cells is the synaptic substrate of memory since the synapse is a functional unit in our brain.

After decades from Hebb’s insight, in the 1970s, a persistent increase of synaptic transmission following strong stimulation was observed in hippocampus and this phenomenon has been called long-term potentiation (LTP) (Bliss and Lømo, 1973). LTP strongly supports that Hebbian plasticity indeed occurs in the mammalian hippocampus (Bliss and Collingridge, 1993). After the finding of LTP, LTP and Hebbian plasticity are accepted as a fundamental synaptic mechanism of memory encoding based on growing evidence demonstrating that the molecular

and cellular mechanisms of LTP and memory are closely related.

Memory engram

Richard W. Semon proposed that memory resided in the engram, which encompasses the physical substrate that is necessary and sufficient for memory expression (Semon, 1921, 1923). After his suggestion, the quest to identify the memory engram, the specific sites of memory storage, has been much focused in the neuroscience field. The early attempts could not success to find memory engram because of the lack of fine techniques. Nowadays, however, using new powerful techniques such as optogenetics and mouse genetics, studies demonstrated that specific populations of neurons are activated during memory formation and necessary and sufficient for memory storage and expression. Thus, it is widely accepted that these specific neuronal populations comprise the engram (Josselyn et al., 2015).

For example, in 2012, Tonegawa's group reported that artificial activation of the neuronal population which activated during learning-induced freezing, a typical expression of fear memory (Liu et al., 2012). After this report, many papers also demonstrated the sufficiency of this neuronal population to memory expression (Cowansage et al., 2014; Ohkawa et al., 2015; Ramirez et al., 2013; Ramirez et al., 2015). In addition, artificial inhibition of neuronal population which activated during learning resulted in a failure of memory expression (Denny et al., 2014; Tanaka et al., 2014). Therefore, specific populations of neurons, which exhibit neuronal activation during memory formation, might be necessary and sufficient for memory expression.

Meanwhile, increased neuronal excitability have a significant role in governing which neurons will participate in the engram. In 2007, Josselyn's group reported that memory could be allocated into CREB overexpressing neurons (Han et al., 2007). After this report, other research has shown that memory could be allocated into neurons with high excitability (Yiu et al., 2014). In addition, the neuronal population with increased excitability has also been demonstrated to be sufficient and necessary for memory expression (Han et al., 2009; Kim et al., 2014; Sano et al., 2014; Yiu et al., 2014; Zhou et al., 2009). Taken together, neuronal ensembles which were activated by learning and/or had increased excitability could be regarded as the engram cells due to its necessity and sufficiency for memory expression (Kim et al., 2016). Based on these findings in the hippocampus and amygdala which is typical brain regions known to be related with memory, memory engram cells have been elucidated in many regions with various types of memory (Figure 2) (Tonegawa et al., 2015).

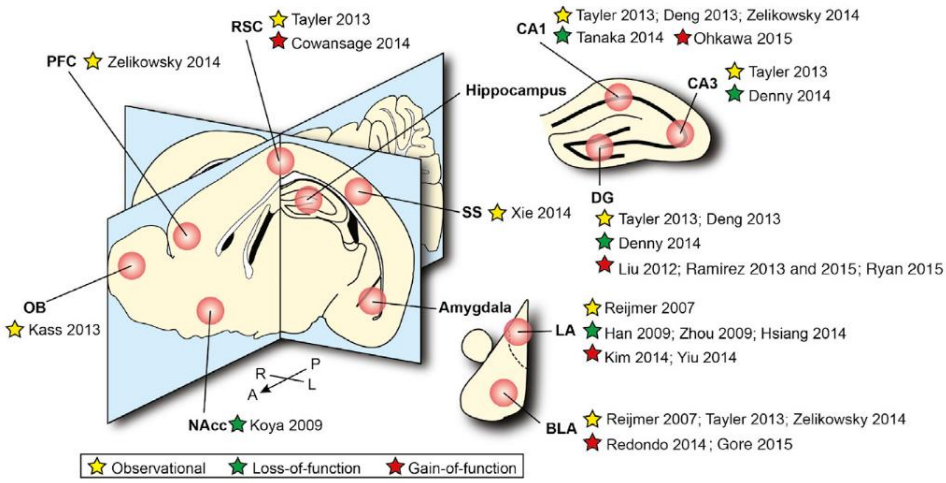

(Adapted from Tonegawa et al., 2015)

Figure 2. Brain regions of memory engram cell populations

Identified memory engram cell populations in various brain regions with different types of supporting evidence (observational, loss of function, and gain of function) of representative studies.

PURPOSE OF THIS STUDY

After the first effort to find the memory engram, now we know that the neuronal population, which show higher excitability and fire during learning, would be included in the memory engram. In other words, recent studies successfully identify the memory engram cells in various brain regions. However, previous studies were limited to neuron-level. Elucidating which synapses would be engram synapses is also crucial to understand the nature of memory because synapse is a functional unit of the nervous system. We do not know the rule of memory allocation in synapse-level since it was impossible to distinguish synapses on one neuron based on their presynaptic population. In this thesis, I developed new synapse-marking technique and applied it to engram study to find the memory engram in synapse-level.

In chapter II, I developed much brighter and dual-color split fluorescent protein-based synapse-marking technique by introducing several mutations and protein-protein interaction domains. Next, I tested whether the fluorescent signal came only from the interface of cell-cell contact and whether different colors (cyan and yellow) could be separated well in vitro system. Then, I applied this technique to mouse brain and confirmed that this tool could distinguish synapses on one dendrite regarding their presynaptic regions.

In chapter III, I applied the technique to the memory engram. I distinguished possible four-types of CA3 to CA1 synapses (between engram to engram, engram to non-engram, non-engram to engram, non-engram to non-engram). Then, I measured the synaptic density and spine morphology to find

synapses modified after memory formation.

In chapter IV, the functional plasticity of four-types of CA3 to CA1 synapses were investigated. I performed a series of electrophysiological experiments to measure the modification of synaptic transmission. To test presynaptic plasticity, I examined the paired-pulse ratio. Next, I examined miniature excitatory postsynaptic currents (mEPSC) to find postsynaptic plasticity. Finally, I induced LTP to find occlusion effect on engram – engram synapses.

Collectively, in this thesis, I defined the synaptic engram by demonstrating that synapses between engram cells specifically undergo synaptic potentiation after memory formation.

CHAPTER II

Development of dual-eGRASP and its application in mouse brain

INTRODUCTION

The synapse is a functional and structural unit of our nervous system. Synaptic transmission is adjusted dynamically depends on external and internal stimuli. Indeed, molecular, structural, and functional changes of synapses regarded as essential mechanisms for various functions (Blair et al., 2001; Bliss et al., 2016; Malenka, 1994; Martin et al., 2000) and malfunctions (Huber et al., 2002; Russo et al., 2010; Selkoe, 2002; Stephan et al., 2009; Wolf, 2016) of brain. Therefore, observing the changes of synapses is strongly emphasized to investigate the synaptic mechanism of learning and memory.

After the first observation of a synapse by electron microscopy (EM) in 1955 (De Robertis and Bennett, 1955; Palay and Palade, 1955), EM provided lots of remarkable results about fine synaptic structure (Briggman and Bock, 2012). However, EM inherently requires time-consuming, labor-intensive processes and is volume limited. To overcome these problems with fluorescence microscopy, labeling synapses with fluorescent proteins (FP) is widely implemented.

Especially, dual components synaptic detection system using split fluorescent protein has been applied to label synaptic interactions between pre and postsynaptic regions (Lee et al., 2016). When Green Fluorescent Protein (GFP) was split into two components (spG1-10 and spG11), the fluorescent signal could be detected only at GFP reconstitution sites. Using this property, split GFP based synapse-labeling technique in mammalian brain such as mammalian Green fluorescent protein Reconstitution Across Synaptic Partners (mGRASP) (Kim et al., 2011) and SynView (Tsetsenis et al., 2014) are developed to mark synapses

between brain regions of interest by expressing one component in presynaptic region and the other component in postsynaptic region. These tools have been contributed to understanding hippocampal structures at synapse-level (Druckmann et al., 2014; Tsetsenis et al., 2014). However, there are clear limitations for wide application. For example, the fluorescent signals are relatively too weak for imaging. Moreover, because it is possible to label only one-color with these techniques, the synapses could not be compared in the same brain regions and neurons.

In this chapter, I modified current synapse labeling techniques and successfully developed dual-enhanced GRASP (eGRASP) technique. To enhance the fluorescent signal from reconstituted split GFP, I introduced protein-protein interaction domains to increase the binding probability of two components of split GFP. In addition, to overcome the one-color system of previous techniques, I developed distinguishable split cyan and yellow fluorescent proteins (CPF and YFP, respectively) using rationally selected mutations. I confirmed this dual-eGRASP works well in vitro system. Finally, I applied dual-eGRASP in mouse brain and confirmed that synapses on one dendrite could be distinguished regarding its presynaptic regions.

EXPERIMENTAL PROCEDURES

Animals

All experiments were performed on 8~10-week-old male C57BL/6N mice purchased from Samtako. Bio. Korea. Mice were raised in 12-hr light/dark cycle in standard laboratory cages and given ad libitum access to food and water. All procedures and animal care were followed the regulation and guidelines of the Institutional Animal Care and Use Committees (IACUC) of Seoul National University.

Construction of cyan and yellow eGRASP

The pre-eGRASP construct consists with an IgG kappa signal peptide, strand 1-10 of the mutant GFP, an Abl SH3 binding peptide, and a neurexin1b stalk, transmembrane and intracellular domain. The strand 1-10 contains an S72A (amino acid numbering based on GFP sequence) mutation additionally to the original GRASP mutations. The cyan pre-eGRASP contains additional T65S, Y66W, H148G, T205S mutations including the S72A mutation, while yellow pre-eGRASP contains S72A and T203Y mutations. The Abl SH3 binding peptide was either p30 (APTKPPPLPP) or p32 (SPSYSPPPPP). The post-eGRASP construct consists with an IgG kappa signal peptide, an Abl SH3 domain, strand 11 of the mutant GFP, and a neuroligin1 stalk, transmembrane and intracellular domain with the last 4 amino acids deleted. The last 4 amino acids of the neuroligin1 which consist the

PDZ domain binding site was deleted to avoid undesired recruitment of scaffolding proteins and receptors. The protein sequence of each construct is listed below.

pre-eGRASP(p30) : IgG kappa signal peptide (orange), strand 1-10 with S72A muation (green with green highlight for S72A), p30 (red), neurexin1b stalk, transmembrane and intracellular domain (blue). (p32 version has a replacement of APTKPPPLPP to SPSYSPPPPP)

METDTLLLWVLLLWVPGSTGDAPVGGSKGEELFTGVVPILVELDGDVNGH
KFSVRGEGEGDATIGKLTLKFICTTGKLPVPWPTLVTTLTYGVQCFARYPD
HMKRHDFFKSAMPEGYVQERTISFKDDGKYKTRAVVKFEGDTLVNRIELK
GTDFKEDGNILGHKLEYNFNSHNVYITADKQKNGIKANFTVRHNVEDGSV
QLADHYQQNTPIGDGPVLLPDNHYLSTQTVLSKDPNEKTGGSGGSGGSRA
PTKPPPLPPGGGSGGGSGTEVPSSMTTESTATAMQSEMSTSIMETTTTLATS
TARRGKPPTKEPISQTTDDILVASAECPSDDEDIDPCEPSSGGLANPTRVGG
REPYPGSAEVIRESSSTTGMVVGIVAAAALCILILLYAMYKYRNRDEGSYH
VDESRNYISNSAQSNGAVVKEKQPSSAKSANKNKKNKDKEYYV

Cyan pre-eGRASP(p30) : IgG kappa signal peptide (orange), strand 1-10 with mutations (green with cyan highlights for cyan-specific mutated amino acids), p30 (red), neurexin1b stalk, transmembrane and intracellular domain (blue). (p32 version has a replacement of APTKPPPLPP to SPSYSPPPPP)

METDTLLLWVLLLWVPGSTGDAPVGGSKGEELFTGVVPILVELDGDVNGH
KFSVRGEGEGDATIGKLTLKFICTTGKLPVPWPTLVTTLSWGVQCFARYPD

HMKRHDFFKSAMPEGYVQERTISFKDDGKYKTRAVVKFEGDTLVNRIELK

GTDFKEDGNILGHKLEYNFNSGNVYITADKQKNGIKANFTVRHNVEDGSV

QLADHYQQNTPIGDGPVLLPDNHYLSTQSVLSKDPNEKTGGSGGSGGSRA

PTKPPPLPPGGGSGGGSGTEVPSSMTTESTATAMQSEMSTSIMETTTTLATS

TARRGKPPTKEPISQTTDDILVASAECPSDDEDIDPCEPSSGGLANPTRVGG

REPYPGSAEVIRESSSTTGMVVGIVAAAALCILILLYAMYKYRNRDEGSYH

VDESRNYISNSAQSNGAVVKEKQPSSAKSANKNKKNKDKEYYV

Yellow pre-eGRASP(p30) : IgG kappa signal peptide (orange), strand 1-10 with mutations (green with Yellow highlights for yellow-specific mutated amino acid), p30 (red), neurexin1b stalk, transmembrane and intracellular domain (blue). (p32 version has a replacement of APTKPPPLPP to SPSYSPPPPP)

METDTLLLWVLLLWVPGSTGDAPVGGSKGEELFTGVVPILVELDGDVNGH

KFSVRGEGEGDATIGKLTLKFICTTGKLPVPWPTLVTTLTYGVQCFARYPD

HMKRHDFFKSAMPEGYVQERTISFKDDGKYKTRAVVKFEGDTLVNRIELK

GTDFKEDGNILGHKLEYNFNSHNVYITADKQKNGIKANFTVRHNVEDGSV

QLADHYQQNTPIGDGPVLLPDNHYLSYQTVLSKDPNEKTGGSGGSGGSRA

PTKPPPLPPGGGSGGGSGTEVPSSMTTESTATAMQSEMSTSIMETTTTLATS

TARRGKPPTKEPISQTTDDILVASAECPSDDEDIDPCEPSSGGLANPTRVGG

REPYPGSAEVIRESSSTTGMVVGIVAAAALCILILLYAMYKYRNRDEGSYH

VDESRNYISNSAQSNGAVVKEKQPSSAKSANKNKKNKDKEYYV

Post-eGRASP : IgG kappa signal peptide (orange), Abl SH3 domain (red), strand 11 (green), neuroligin1 stalk, transmembrane and intracellular domain with deletion (blue).

METDTLLLWVLLLWVPGSTGDAPVGGNDPNLFVALYDFVASGDNTLSITK
GEKLRVLGYNHNGEWCEAQTKNGQGWVPSNYITPVNSTGGGSGGGSGRD
HMVLHEYVNAAGITGGGSGGGSGTLELVPHLHNLNDISQYTSTTTKVPST
DITLRPTRKNSTPVTSAFPTAKQDDPKQQPSPFSVDQRDYSTELSVTIAVGA
SLLFLNILAFAALYYKKDKRRHDVHRRCSPQRTTTNDLTHAPEEEIMSLQM
KHTDLDHECESIHPHEVVLRTACPPDYTLAMRRSPDDIPLMTPNTITMIPNT
IPGIQPLHTFNTFTGGQNNTLPHPHPHPHSHS

AAV production

Adeno-Associated Viruses serotype 1/2 (AAV1/2; AAV particle that contains both serotype 1 and 2 capsids) were used in all the experiments. AAV1/2s were purified from HEK293T cells that were transfected with plasmids containing each expression cassette flanked by AAV2 ITRs, p5E18, p5E18-RXC1 and pAd-ΔF6 and cultured in 18 ml or 8 ml Opti-MEM (Gibco-BRL/Invitrogen, cat# 31985070) in a 150-mm or 100-mm culture dish, respectively. Four days after transfection, the medium containing AAV1/2 particles was collected and centrifuged at 3,000 rpm for 10 min. After 1 ml of heparin-agarose suspension (Sigma, cat# H6508) was loaded onto a poly-prep chromatography column (Bio-Rad Laboratories, Inc. cat# 731-1550), the supernatant was loaded onto the column carefully. The column was washed by 4 ml of Buffer 4-150 (150 mM NaCl, pH4 10 mM citrate buffer) and 12 ml of Buffer 4-400 (400 mM NaCl, pH4 10 mM

citrate buffer). The virus particles were eluted by 4 ml of Buffer 4-1200 (1.2 M NaCl, pH4 10 mM citrate buffer). The eluted solution was exchanged with PBS and concentrated using an Amicon Ultra-15 centrifugal filter unit (Millipore, cat# UFC910024). The titer was measured using quantitative RT-PCR.

Stereotaxic surgery

Mice (8~10 weeks) were anesthetized with a ketamine/xylazine solution and positioned in a stereotaxic apparatus (Stoelting Co.). The viruses were injected using 33 gauge needle with Hamilton syringe at a 0.1 μl/min rate into target regions. At all injected points, the tip of the needle was positioned 0.05mm below the target coordinate and returned to the target site after 2min. After injection, the needle stayed in place for an additional 7 mins and was withdrawn slowly. Stereotaxic coordinates for each target sites are lateral entorhinal cortex (AP: -3.4/ ML: -4.4/ DV: -4.1), medial entorhinal cortex (AP: -4.6/ ML:-3.5/ DV-3.5), DG (AP: -1.75/ ML: -1.5/ DV: -2.2 below from skull surface), CA3 (AP: -1.9/ ML: ±2.35/ DV: -2.45) and CA1 (AP: -1.9/ ML: -1.5/ DV: -1.6).

RESULTS (Collaborated with Dr. Jun-Hyeok Choi)

Enhancing fluorescent signal by introducing protein-protein interaction domains and a single mutation

To overcome the limitations of current synapse labeling techniques and compare synapses on a single postsynaptic neuron according to their different presynaptic populations, I modified the GRASP technique (Kim et al., 2011; Lee et al., 2016). Because GRASP signals are generally too weak, I first planned to develop the enhanced GRASP (eGRASP) technique, which exhibits enhanced intensity by adding a weakly interacting domain that facilitates reconstitution (Fig. 3). After introducing peptide p40 (APTYSPPPPP) into pre GRASP construct and SH3 domain into post GRASP construct, the fluorescent signal from GRASP was markedly enhanced (Fig. 3A). Since additional binding domains might be able to make physical forces that induce abnormal effects on synaptic morphology, I exchanged the SH3 binding peptide with lower interacting strengths. I confirmed that GRASP with lower interacting domains still showed a significant fluorescent signal compared to mGRASP (Fig. 3B).

In addition, I also introduced a single mutation commonly found on most advanced GFP variants (Pisabarro and Serrano, 1996). This single mutation could further enhance the fluorescent signal (Fig. 4A). This eGRASP technique with the enhanced fluorescent signal using newly introduced protein-protein interaction domains and a single mutation showed markedly clear signals on the spines of CA1 dendrites even with the weakest interacting peptide while mGRASP signal was not detectable in my condition (Fig. 4B).

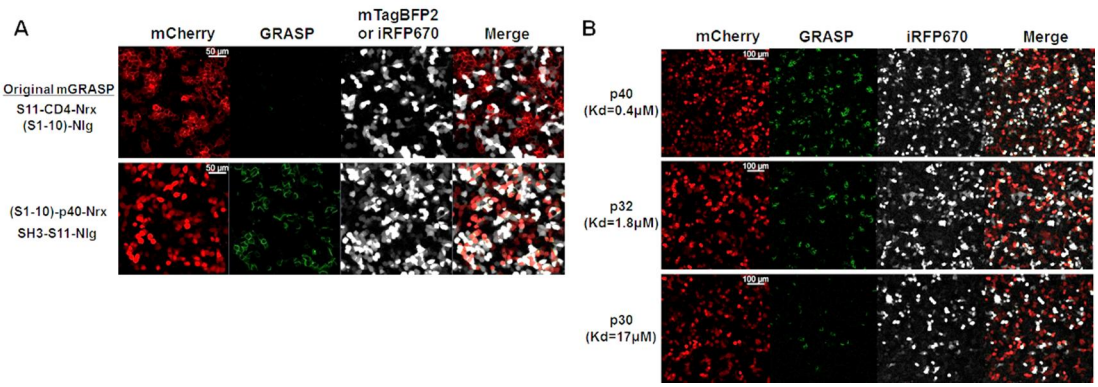

Figure 3. Enhancement of GRASP signal with protein-protein interaction domains

(in collaboration with Dr. Jun-Hyeok Choi)

(A) (Top) Either post-mGRASP with mTagBFP2 coexpression or pre-mGRASP with mCherry fusion was transfected separately in HEK293T cells by nucleofection. The interface of mCherry positive cell and mTagBFP2 positive cell shows only faint GRASP signal, only detectable when exposed to stronger excitation. (Bottom) Either post-eGRASP (SH3-S11-Nlg) with iRFP670 coexpression or (S1-10)-p40-Nrx with mCherry coexpression was transfected separately in HEK293T cells by nucleofection. The interface of a mCherry positive cell and an iRFP670 positive cell shows strong GRASP signal.

(B) Exchanging the SH3 binding peptide to those with lower interacting strength reduces the GRASP signal, while still showing significant GRASP signal compared to mGRASP. The known dissociation constants for SH3 domain and each peptide are indicated below the peptide.

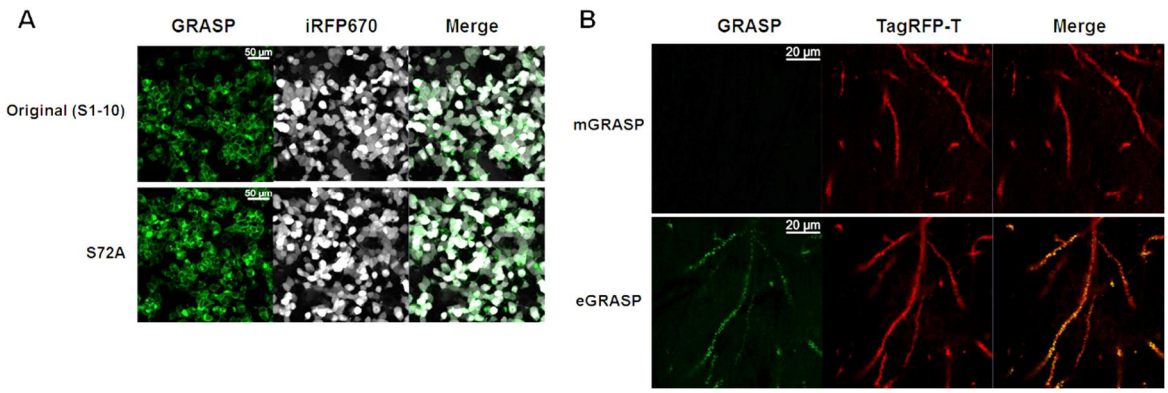

Figure 4. Enhancement of GRASP signal with a single mutation

(in collaboration with Dr. Jun-Hyeok Choi)

(A) Additional S72A mutation on the strand 1-10 of the split GFP increased the GRASP signal.

(B) (Top) pre-mGRASP was expressed in the CA3 and post-mGRASP with membrane-targeted TagRFP-T was expressed sparsely in CA1. (Bottom) pre-eGRASP with the weakest interacting peptide (p30) was expressed in CA3 and post-eGRASP with membrane-targeted TagRFP-T was expressed sparsely in CA1.

Development of distinguishable dual-color fluorescent signal with rationally selected mutations

Previous techniques based on split GFP could mark synapses as only single excitation/emission wavelength. To overcome this problem, I developed eGRASP into dual-color system by perfectly distinguishable split CFP and split YFP with a series of rationally selected mutations. First, mutations that make emission and excitation wavelength of fluorescent protein shifted to violet were serially introduced. Relatively bright cyan eGRASP signal could be obtained with T65S, Y66W, S72A, H148G, T205S mutations (Fredj et al., 2012; Goedhart et al., 2012; Köker et al., 2018; Sawano and Miyawaki, 2000) (Fig. 5A). In addition, a bright yellow eGRASP signal obtained from pre-eGRASP with S72A, T203Y mutations (Köker et al., 2018). This eGRASP signal detected in both the GFP and YFP filters, but not in the CFP filter (Fig. 5B). Collectively, I developed much brighter and perfectly distinguishable dual-eGRASP by introducing protein-protein interaction domains and series of rationally selected mutations (Fig. 5C).

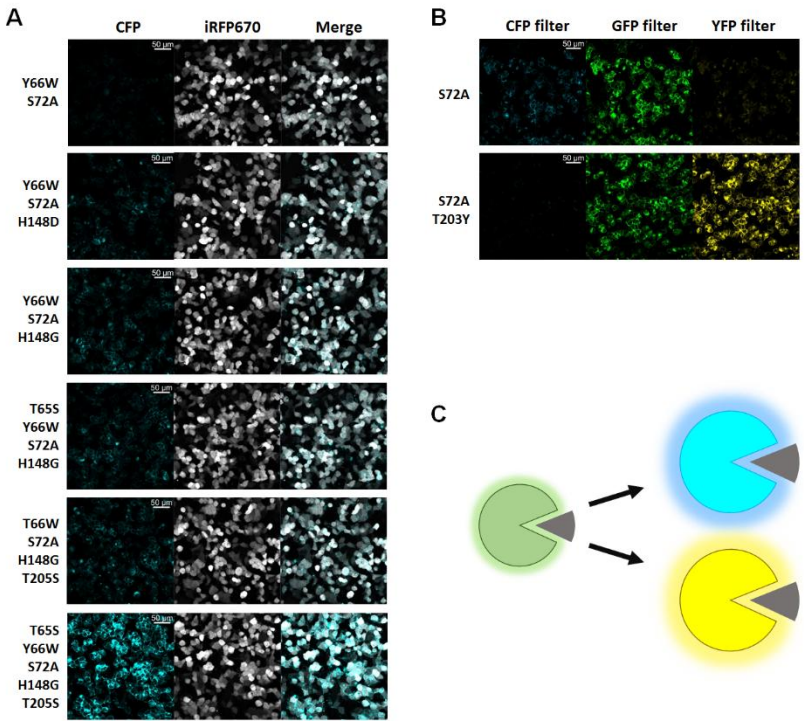

Figure 5. Development of cyan and yellow eGRASP

(in collaboration with Dr. Jun-Hyeok Choi)

(A) Pre-eGRASP with indicated mutations, post-eGRASP and iRFP670 were coexpressed in HEK293T cells. Pre-eGRASP that contains T65S, Y66W, S72A, H148G, T205S shows the brightest cyan fluorescence.

(B) Pre-eGRASP with indicated mutations, post-eGRASP and iRFP670 were coexpressed in HEK293T cells. Pre-eGRASP that contains S72A, T203Y shows bright signal detected in both the GFP and YFP filters, but not in the CFP filter. The original pre-eGRASP shows signal using every filter with the GFP filter being the brightest. This indicates that the T203Y mutation results in red-shifted fluorescence that is separable from the CFP signal.

(C) Schematic illustration showing the development of cyan and yellow shifted fluorescence and brighter pre-eGRASP.

Application of dual-eGRASP in vitro

By expressing cyan or yellow pre-eGRASP with post-eGRASP in HEK293T cells, I confirmed that fluorescent signal from cyan eGRASP was only detected in CFP filter, but not in YFP filter, vice versa. That is, cyan and yellow eGRASP did not be overlapped and could be imaged separately (Fig. 6A). In addition, I could identify the contact interface of HEK293T cells expressing the common domain with cells expressing the color-determining domain with two colors (Fig. 6B).

After the validation of brightness and duality of dual-eGRASP in HEK293T cells, this also was applied to label synapses like the schematic illustration (Fig. 7). Placing the color-determining domain in the complementary GFP fragment to the presynaptic neuron (cyan/yellow pre-eGRASP) and the common domain to the postsynaptic neuron (post-eGRASP) enabled the visualization of two synaptic populations that originated from different presynaptic neuron populations in one neuron.

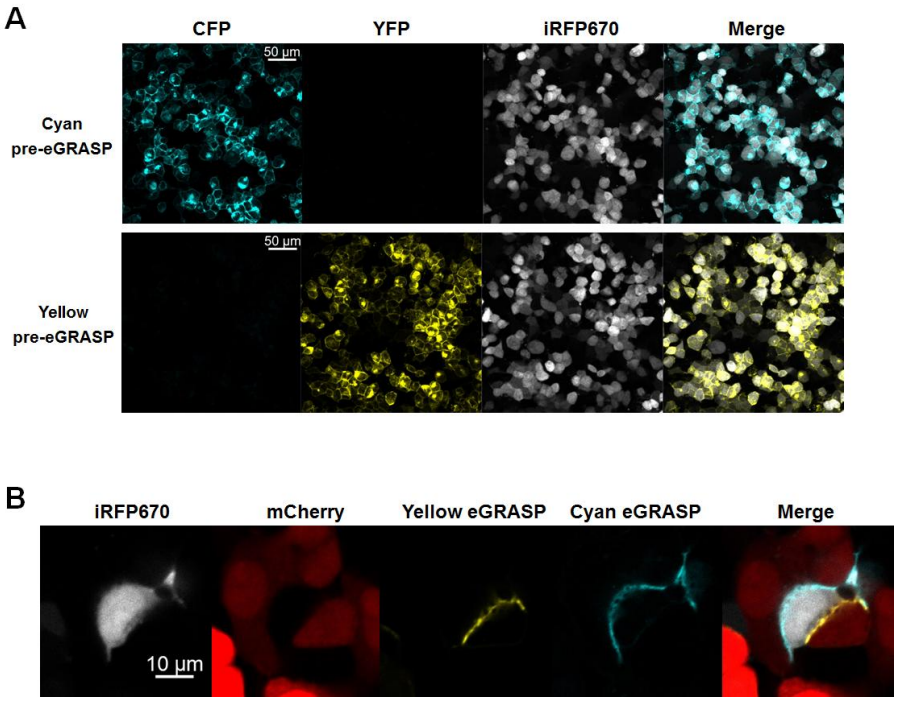

Figure 6. Bright and distinguishable dual-eGRASP signals in vitro system

(in collaboration with Dr. Jun-Hyeok Choi)

(A) Post-eGRASP and iRFP670 were coexpressed with either cyan or yellow pre-eGRASP in HEK293T cells.

(B) Interaction contact of one HEK293T cell with other cells showed either cyan or yellow fluorescent signals that were completely distinguishable.

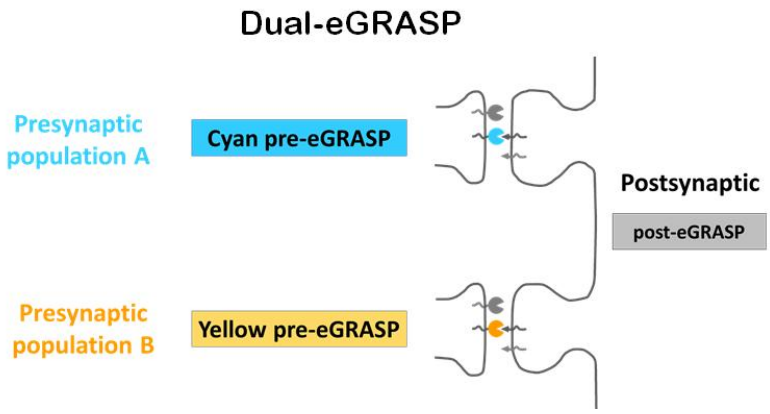

Figure 7. Schematic illustrations of dual-eGRASP

Schematic illustrations of cyan and yellow eGRASP. Cyan pre-eGRASP and yellow pre-eGRASP are expressed in two different presynaptic population, while common post-eGRASP is expressed in a single postsynaptic cell.

Dual-eGRASP enabled discrimination of synapses originated from different presynaptic neuronal populations

Next, to test whether dual-eGRASP technique successfully applied in mouse brain, pre-eGRASP and post-eGRASP constructs were expressed in various mouse brain regions using AAVs. To achieve sparse but strong expression of fluorescent signal from dendrites to track easily, EF1α promoter-driven Cre-dependent post-eGRASP and myr_TagRFP-T (myrTRT) was injected with low titers of CaMKIIα promoter-driven iCre-expressing AAV (Fig. 8A). First, I applied dual-eGRSAP to identify synapses on DG granule cells because it is well known that granule cells receive input from either the lateral entorhinal cortex (LEC) or medial entorhinal cortex (MEC) projecting to the DG outer and middle molecular layers, respectively (Amaral et al., 2007). As a result, Cyan and yellow eGRASP signals were clearly distinguishable in dendrites of DG granule cells (Fig. 8B).

In addition, I could also separately label intermixed synapses originated from either the contralateral CA3 or ipsilateral CA3 that do not have a unique spatial distribution on CA1 pyramidal neurons (Fig. 9) (Finnerty and Jefferys, 1993). These results show that dual-eGRASP successfully discriminated synapses innervated from different presynaptic neuronal populations in the rodent brain.

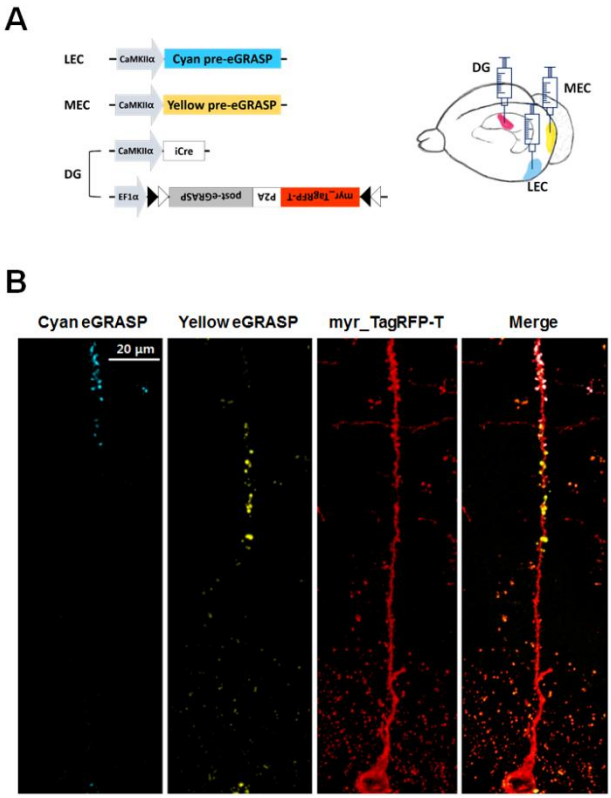

Figure 8. Dual-eGRASP distinguish synapses on one granule cell in DG from LEC or MEC

(A) (Left) Schematic illustrations of injected AAVs. (Right) Schematic illustration of injected brain sites.

(B) In LEC and MEC, Cyan pre-eGRASP and yellow pre-eGRASP were expressed respectively by stereotaxic virus injection. Myristoylated TagRFP-T (myr_TagRFP-T) were expressed in the DG with post-eGRASP. Cyan and yellow puncta were clearly distinguishable in the dendrite of one DG granule cell.

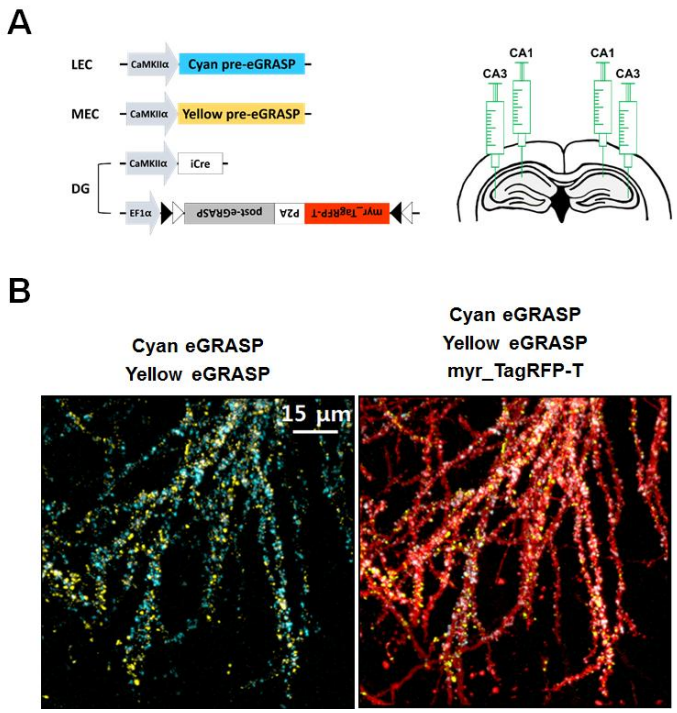

Figure 9. Dual-eGRASP distinguish synapses on one pyramidal neuron in CA1 from CA3 in different hemispheres

(A) (Left) Schematics of injected AAVs. (Right) Schematic illustration of injected brain sites.

(B) Cyan pre-eGRASP were expressed in right CA3 and yellow pre-eGRASP were expressed in left CA3, respectively. Myr_TagRFP-T were expressed in CA1 together with post-eGRASP. Dendrites of CA1 pyramidal cells show clearly distinguishable cyan and yellow puncta.

Effect of dual-eGRASP on synaptic transmission

To test whether dual-eGRASP affects on synaptic transmission and induces undesired effects on synapses, I examined mEPSCs of CA1 neurons from hippocampal slices, which expressed pre- and post-eGRASP constructs.

I compared amplitude and frequency of mEPSC from hippocampal slices which expressed post-eGRASP only in CA1, pre-eGRASP only in CA3, both pre- and post-eGRASP in CA3 and CA1 respectively, and also which did not express any eGRASP constructs. I confirmed that the reconstitution of eGRASP did not induce abnormal strengthening of the synaptic transmission between the neurons expressing pre-eGRASP and post-eGRASP (Fig. 10).

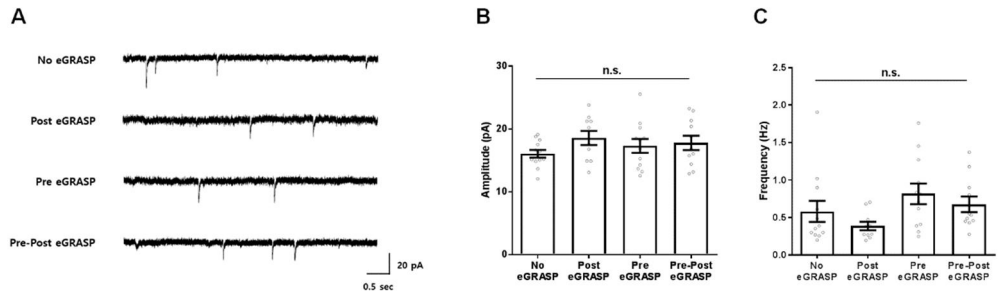

Figure 10. Expression of dual-eGRASP components has no effects on basal synaptic transmission

(in collaboration with Dr. Su-Eon Sim)

(A) Representative mEPSC recording traces.

(B and C) Amplitude and frequency of mEPSCs from CA1 pyramidal neurons in slices expressing eGRASP components in CA3 and CA1 as indicated in each group. No eGRASP (no eGRASP components in both CA3 and CA1), n = 12; Post eGRASP (post-eGRASP in CA1), n = 10; Pre eGRASP (pre-eGRASP in CA3), n = 12; Pre-Post eGRASP (pre-eGRASP in CA3 and post-eGRASP in CA1), n = 11. One-way ANOVA of amplitude, n.s.: not significant, $F(3,41) = 1.074$, $p = 0.3705$. One-way ANOVA of frequency, n.s.: not significant, $F(3,41) = 2.167$, $p = 0.1065$. Data are represented as mean ± SEM.

DISCUSSION

In this chapter, I developed dual-eGRASP, which is a novel synapse-labeling technique, with enhanced fluorescent signals and distinguishable cyan and yellow colors. In particular, the duality of this new technique makes possible to compare the synapses within one dendrite regarding the presynaptic regions.

Various neuroscience fields can utilize dual-eGRASP, especially for connectomics studies. Connectomics is the study of connectomes: defining of comprehensive structures of networks within an organism's nervous system. The goal of connectomics is the mapping the complex connectivity graph (Helmstaedter, 2013). Despite the many issues about making the connectome, it is widely accepted that mapping the complex brain structure will help neuroscientists in many aspects (Morgan and Lichtman, 2013). However, there are many hurdles to be overcome for achieving the goal of connectomics. For instance, identifying synapses, and more importantly, tracking the presynaptic and postsynaptic neurons are big challenges for cellular connectomics based on EM images (Helmstaedter, 2013). Since dual-eGRASP can distinguish synapses on a single dendrite innervated from two different and identified regions, I wish that this approach might become a breakthrough for wiring the connections between neurons. In addition, when cyan and yellow pre-eGRASP are expressed under the promoters of cell-type specific markers, it is possible to mapping the structure of synapses on one dendrite regarding the cell types (such as excitatory vs inhibitory neurons) of the presynaptic neurons even if the presynaptic neurons are in the one region.

Therefore, dual-eGRASP might provide more sophisticated connectome analyses when applied to multiple brain regions.

In addition, split fluorescent proteins, as well as split protein reconstitution systems, have been widely used for many purposes such as studying protein-protein interactions (Shekhawat and Ghosh, 2011). There are open chances that these already developed split protein systems could be applied into neuroscience field to understand synaptic mechanisms. The efforts of this chapter to enhance the reconstitution of split fluorescent proteins by introducing protein-protein interaction domains might give help to increase the reconstitution of any split proteins.

CHAPTER III

Increased synapse number and spine size between CA3 engram and CA1 engram cells after memory formation

INTRODUCTION

Using newly developed synaptic labeling technique, dual-eGRASP, I next focused on finding the synaptic engram through defining the changes of structural connectivity between engram cells. After Richard W. Semon's suggestion that memory resided in the memory engram (Semon, 1921, 1923), many studies found engram cells throughout various brain regions and demonstrated that activation of engram cells induced artificial retrieval of memories (Denny et al., 2014; Han et al., 2009; Liu et al., 2012; Ramirez et al., 2013; Tanaka et al., 2014; Zhou et al., 2009).

Despite these brilliant achievements to find the memory engram, we do not know the synaptic changes between engram cells. Because the enhancement of synapses is a fundamental mechanism of memory encoding as Hebb proposed (Hebb, 1949), it is important to study whether memory formation strengthens or enhances synapses between engram cells in different brain regions. However, we could only study the engram at the neuronal level, not the synaptic level, since it was impossible to distinguish which synapses originate from engram cells in presynaptic regions.

In this chapter, I used dual-eGRASP to demonstrate that synapses between CA3 engram cells and CA1 engram cells show enhanced structural connectivity after memory formation. First, I validated Fos-rtTA system to express dual-eGRASP components in activity- and doxycycline-dependent manner. Combining Fos-rtTA system and dual-eGRASP technique, I differentiated four synapse types (engram to engram, engram to non-engram, non-engram to engram, non-engram to non-engram) at CA3-CA1 connections.

EXPERIMENTAL PROCEDURES

Animals

All experiments were performed on 8~10-week-old male C57BL/6N mice purchased from Samtako. Bio. Korea. Mice were raised in 12-hr light/dark cycle in standard laboratory cages and given ad libitum access to food and water. All procedures and animal care followed the regulation and guidelines of the Institutional Animal Care and Use Committees (IACUC) of Seoul National University.

Construction of Fos-rtTA system

Temporally-controlled activity-dependent transgene expression used a Fos promoter driven rtTA3G with an additional AU-rich element of Fos mRNA, which induced rapid destabilization of the mRNA following the rtTA3G. The transgenes of interest were driven by a TRE3G promoter, making it both rtTA3G expression- and doxycycline-dependent.

AAV production

Adeno-Associated Viruses serotype 1/2 (AAV1/2; AAV particle that contains both serotype 1 and 2 capsids) were used in all the experiments. AAV1/2s were purified from HEK293T cells that were transfected with plasmids containing each expression cassette flanked by AAV2 ITRs, p5E18, p5E18-RXC1 and pAd-

ΔF6 and cultured in 18 ml or 8 ml Opti-MEM (Gibco-BRL/Invitrogen, cat# 31985070) in a 150-mm or 100-mm culture dish, respectively. Four days after transfection, the medium containing AAV1/2 particles was collected and centrifuged at 3,000 rpm for 10 min. After 1 ml of heparin-agarose suspension (Sigma, cat# H6508) was loaded onto a poly-prep chromatography column (Bio-Rad Laboratories, Inc. cat# 731-1550), the supernatant was loaded onto the column carefully. The column was washed by 4 ml of Buffer 4-150 (150 mM NaCl, pH4 10 mM citrate buffer) and 12 ml of Buffer 4-400 (400 mM NaCl, pH4 10 mM citrate buffer). The virus particles were eluted by 4 ml of Buffer 4-1200 (1.2 M NaCl, pH4 10 mM citrate buffer). The eluted solution was exchanged with PBS and concentrated using an Amicon Ultra-15 centrifugal filter unit (Millipore, cat# UFC910024). The titer was measured using quantitative RT-PCR.

Stereotaxic surgery

Mice (8~10 weeks) were anesthetized with a ketamine/xylazine solution and positioned in a stereotaxic apparatus (Stoelting Co.). The virus was injected using 33 gauge needle with Hamilton syringe at a 0.1 μl/min rate into target regions. At all injected points, the tip of the needle was positioned 0.05mm below the target coordinate and returned to the target site after 2min. After injection, the needle stayed in place for an additional 7 mins and was withdrawn slowly. Stereotaxic coordinates for each target sites are left CA3 (AP: -1.75/ ML: -2.35/ DV: -2.45) and right CA1 (AP: -1.8/ ML: +1.5/ DV: -1.65 below the skull surface).

0.5 μl of a mixture of viruses ($1.6x10^6$ viral genome (vg)/μl of Fos-rtTA3G, $2.0x10^8$ vg/μl of TRE3G-Yellow pre-eGRASP, $4.0x10^7$ vg/μl of CaMKIIα-iCre, and $7.5x10^8$ vg/μl of EF1α-DIO-Cyan pre-eGRASP) was injected into left CA3. 0.5 μl of a mixture of viruses ($1.6x10^6$ vg/μl of Fos-rtTA3G, $8.0x10^9$ vg/μl of TRE3G-myr_mScarlet-I-P2A-post-eGRASP, $1.0x10^6$ vg/μl of CaMKIIα-iCre, $8.0x10^8$ vg/μl of EF1α-DIO-myr_iRFP670-P2A-post-eGRASP) was injected into right CA1.

Contextual fear conditioning

All mice were conditioned 2~4 weeks after the AAV injection. Each mouse was single caged 10 days before conditioning and was habituated to the hands of the investigator and anesthesia chamber without isoflurane for 3 minutes on each of 7 consecutive days. Mice were conditioned 2 days after the last habituation day. On the conditioning day, 250 μl of 5 mg/ml Doxycycline solution dissolved in saline was injected by intraperitoneal injection during brief anesthesia by isoflurane in the anesthesia chamber 2 hours prior to the conditioning. Conditioning sessions were 300s in duration, and three 0.6 mA shocks of 2 s duration were delivered at 208 s, 238 s, and 268 s from the initiation of the session in a square chamber with a steel grid (Med Associates Inc., St Albans, VT). When the conditioning was finished, mice were immediately transferred to their homecage. 2 days after the conditioning, mice were carefully perfused for eGRASP signal analysis.

Sample preparation and confocal imaging

Perfused brains were fixed with 4% paraformaldehyde (PFA) in PBS overnight at 4℃ and dehydrated in 30% sucrose in PBS for 2 days at 4℃. After freezing, brains were sliced into 50 μm sections by Cryostat and mounted in VECTASHIELD mounting medium (Vector Laboratories) or Easy-index mounting medium (Live Cell Instrument). CA1 apical dendritic regions of the brain slices were imaged by Leica SP8 or Zeiss LSM700 confocal microscope with 63x objectives with distilled water immersion. Secondary/tertiary dendrites of CA1 neurons were imaged in Z-stack.

Image analysis

Imaris (Bitplane, Zurich, Switzerland) software was used to reconstruct 3D models of the confocal images. Each trackable myr_mScarlet-I-positive, myr_mScarlet-I-positive or myr_iRFP670-positive dendrite was denoted as a filament manually while hiding other three channels to exclude any bias, and each cyan or yellow eGRASP signal was denoted as cyan or yellow sphere automatically. When the cyan and yellow eGRASP signals overlapped in a single synapse, it was denoted as a yellow spot as the presynaptic neuron of the synapse indicating IEG-positive during memory formation. Also, if a dendrite did not have any cyan

eGRASP or if the myr_mScarlet-I and myr_iRFP670 signal overlapped in a single dendrite, the dendrite was not denoted as a filament for more accurate analysis.

For eGRASP density analysis, the numbers of denoted cyan and yellow spheres were manually counted along each denoted filaments. The length of each dendrite was measured using Imaris FilamentTracer. Cyan and yellow eGRASP density of each dendrite were normalized to the average density of the cyan and yellow eGRASP on the myr_iRFP670-positive dendrites, respectively, in each image. After denoting the trackable dendrites and eGRASP signals in the same way, eGRASP signal positive spines on denoted dendrites were reconstructed as 3D models and were measured using Imaris FilamentTracer. The investigator who reconstructed the spine 3D models was unaware of the color of the eGRASP signals.

Statistical analysis

Data were analyzed using Prism software. Mann Whitney two-tailed test and Tukey's multiple comparison tests after one-way ANOVA were used to test for statistical significance when applicable. The exact value of n and statistical significance are reported in each figure legends.

RESULTS (collaborated with Dong Il Choi)

Validation of Fos-rtTA system using seizure and contextual fear conditioning

I used a reverse tetracycline-controlled transactivator (rtTA) under Fos promoter to express specific genes of interest in the engram cells (Haasteren et al., 2000; Loew et al., 2010; Reijmers et al., 2007; Zhou et al., 2006). First, I checked the Fos-rtTA system whether a gene of interest could be expressed in activity-dependent manner using chemically induced seizure. Nucleus-targeted mEmerald (mEmerald-Nuc) was driven by the TRE3G promoter controlled by Fos promoter-driven rtTA3G. CaMKIIα driven nucleus targeted mCherry was used as an expression control (Fig. 11A). 2 weeks after virus injection, Pentylenetetrazol (PTZ) was injected intraperitoneally to induce seizure (Fig. 11B). As a result, Doxycycline injection 2 hrs before seizure induction successfully labeled cells that activated during these events (Fig. 11C).

In addition, Fos-rtTA system in CA1 and CA3 cells were also validated using contextual fear conditioning using the same way. Many activity-dependent labeling systems have demonstrated the increased Fos-driven expression after learning event relative to homecage controls (Liu et al., 2012; Reijmers et al., 2007; Tayler et al., 2013). As consistency with these studies, mEmerald-Nuc expression was significantly increased after fear conditioning in the CA3, and a strong tendency of the increase was observed in the CA1 using Fos-rtTA system (Fig. 12). Therefore, I decided to use Fos-rtTA system for specific labeling of engram cells, which are activated population during learning event.

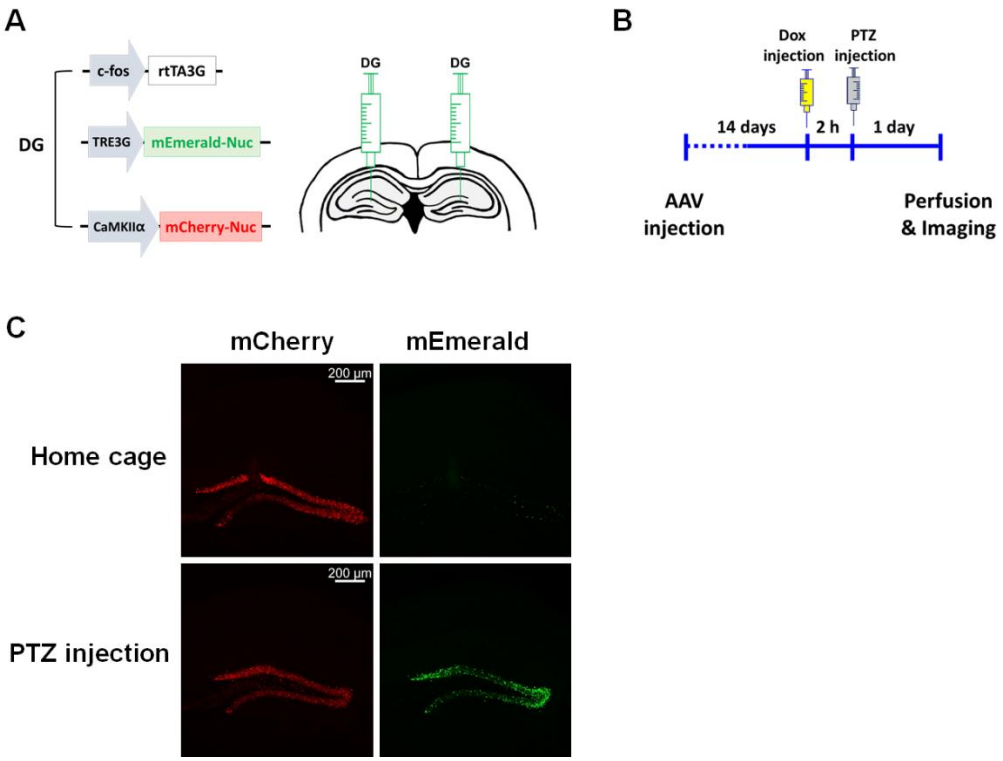

Figure 11. Validation of Fos-rtTA system on seizure

(A) Schematic illustration of injected AAVs and brain sites.

(B) Behavioral schedule used in the experiment.

(C) Seizure-inducing Pentylenetetrazol (PTZ) injection induced a strong mEmerald-Nuc signal in the DG.

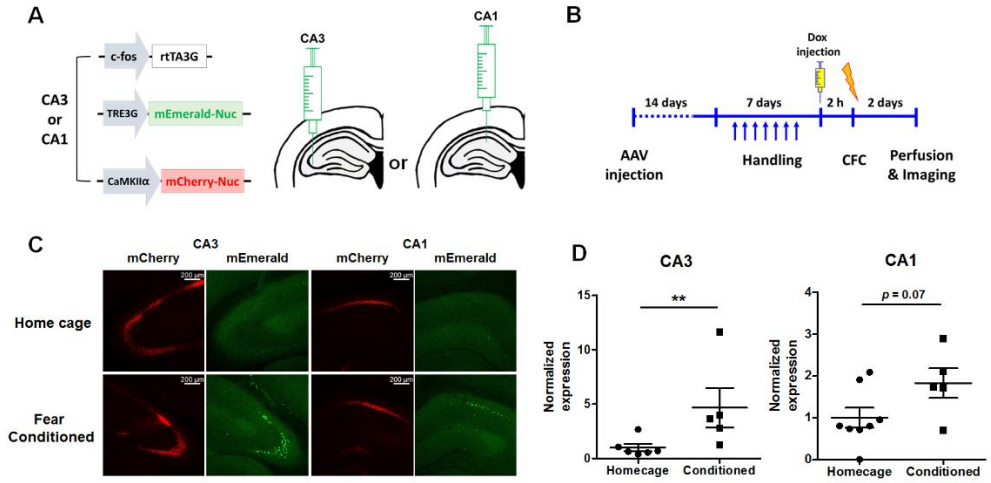

Figure 12. Validation of Fos-rtTA system on contextual fear conditioning

(A) Schematic illustration of injected AAVs and brain sites.

(B) Behavioral schedule used in the experiment.

(C) Representative images.

(D) Fear conditioning induced a significant increase of mEmerald-Nuc in the CA3 and a strong tendency of increase in the CA1. n = 6, CA3 Homecage; n = 5, CA3 Conditioned; n = 8, CA1 Homecage; n = 5, CA1 Conditioned. Unpaired two-tailed t test, **p < 0.01. Data are represented as mean ± SEM.

Strategy for comparison of the four types of synapses between CA3 and CA1

To compare CA3 engram to CA1 engram (E-E) synapses with other types of synapses (non-engram to engram (N-E), engram to non-engram (E-N) and non-engram to non-engram (N-N) synapses), each type of synapses should be distinguished based on whether their presynaptic and postsynaptic neurons are engram or not. To distinguish the synapses, I used dual-eGRASP with Fos-rtTA system.

To label E-E synapses, I expressed post-eGRASP with myristoylated mScarlet-I (Bindels et al., 2017) unilaterally in CA1 engram cells and yellow pre-eGRASP in the contralateral CA3 engram cells to avoid possible coexpression of pre-eGRASP and post-eGRASP. Then, E-E synapses could be marked as yellow eGRASP signals on mScarlet-I labeled dendritic spines. In addition, I expressed post-eGRASP together with myristoylated iRFP670 (Shcherbakova and Verkhusha, 2013) in a sparse neuronal population from the ipsilateral CA1, while expressing cyan pre-eGRASP in a random neuronal population from the contralateral CA3 (Fig. 13A). I achieved these expression patterns using a mixture of various virus constructs. In CA3, yellow pre-eGRASP was driven by the TRE3G promoter controlled by Fos promoter-driven rtTA3G. EF1α promoter-driven Cre-dependent cyan pre-eGRASP was injected with low titers of CaMKIIα promoter-driven iCre-expressing AAV. In the contralateral CA1, unilateral post-eGRASP and myr_mScarlet-I were driven by the TRE3G promoter controlled by Fos promoter-driven rtTA3G. EF1α promoter-driven Cre-dependent post-eGRASP and

myr_iRFP670 were injected with low titers of CaMKIIα promoter-driven iCre-expressing AAV. In this strategy, strong expression in the random, sparse neuronal population was achieved by using a high titer of Double-floxed Inverted pen reading frame (DIO) AAV with a lower titer of Cre recombinase expressing AAV (Fig. 13 B and C).

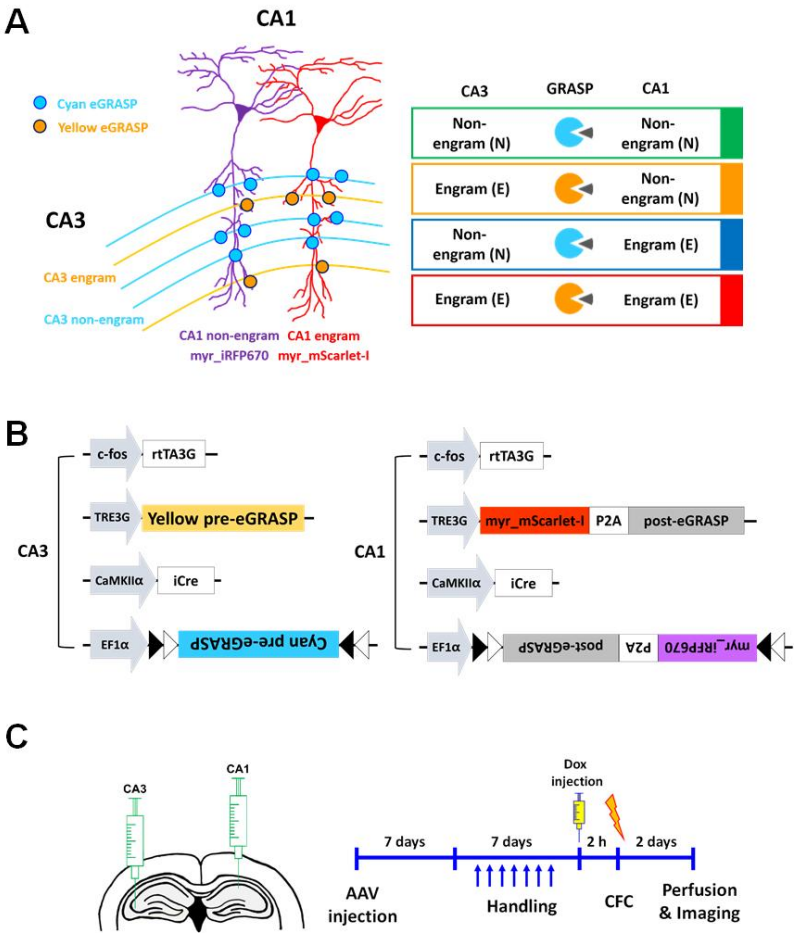

Figure 13. Strategy to compare synapses between engram cells with other types of synapses using dual-eGRASP

(A) (Left) Schematics of the four possible synapse populations among engram and non-engram cells. Cyan circles representing cyan eGRASP signal indicate synapses originating from CA3 non-engram cells. The orange circles representing yellow eGRASP signals indicate synapses originating from CA3 engram cells. CA1 non-engram and engram cells filled with purple and red, respectively. (Right) Classification of the four synaptic populations indicated

by four colors. Green, N-N; Orange, E-N; Blue, N-E; Red, E-E. The color for each group applies to entire figures of Chapter III and Chapter IV.

(B) Schematic illustration of injected AAVs.

(C) (left) Illustration of virus injection site. Injection in each site was performed with a complete cocktail of the entire viruses infected in each site. (Right) Schematic of the experimental protocol.

Successful discrimination of the synapses between CA3 and CA1 engram cells via dual-eGRASP

Using strategy described above, I successfully discriminated four types of synapses in the same brain slice after CFC. I could achieve clear images containing distinguishable fluorescent cyan eGRASP, yellow eGRASP, myr_mScarlet-I and myr_iRFP670 signals which are adequate to be analyzed (Fig. 14). For quantitative analysis, I made 3D modeling of this components using Imaris program. Cyan and yellow eGRASP signals were modeled as cyan and yellow spheres, respectively. myr_mScarlet-I and myr_iRFP670 dendrites were traced as red and white filaments, respectively. Cyan and yellow puncta on mScarlet-I positive dendrites indicated N-E and E-E synapses, respectively, while cyan and yellow puncta on iRFP670 positive dendrites indicated N-N and E-N synapses (Fig. 14). When the cyan and yellow eGRASP signals were overlapped in a single synapse, it was denoted as a yellow spot as the presynaptic neuron of the synapse would be IEG-positive during memory formation.

To confirm the reliability of yellow pre-eGRASP expression under the Fos-rtTA system, I validated whether yellow pre-eGRASP expression was doxycycline-dependent (Fig. 15). This result showed that this system using eGRASP technique could label synapses originating from engram cells of a specific event.

I estimated CA3 cells expressing cyan pre-eGRASP, yellow pre-eGRASP, CA1 cells expressing iRFP and mScarlet-I to be 78.38 %, 40.25 %, 11.61 %, and 20.93 % respectively based on the percentage of overlapping fluorescence (Fig. 16).

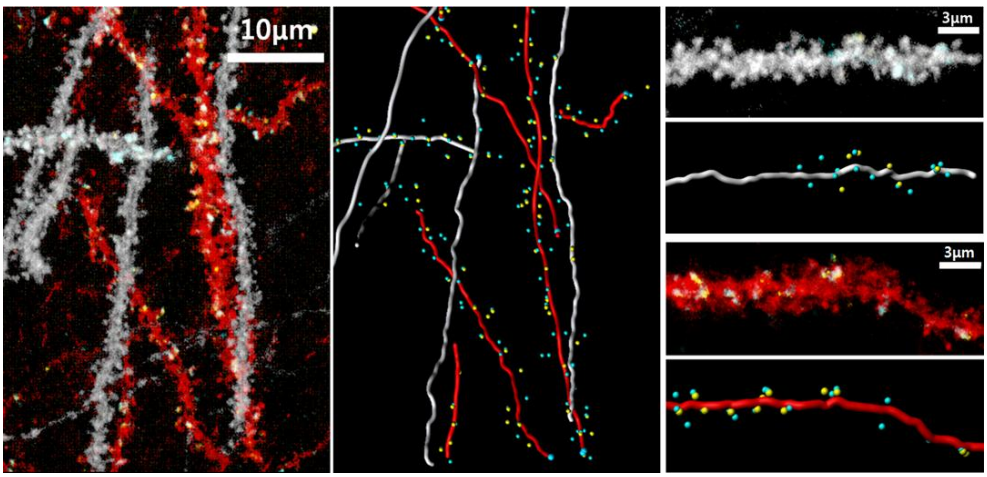

Figure 14. Representative images with 3D modeling for analysis

Dendrites of CA1 engram or non-engram cells were demonstrated by myr_mScarlet-I or myr_iRFP670, respectively. Each dendrite were reconstructed as filaments. Synapses input from CA3 engram cells were labeled by yellow eGRASP signal, and cyan eGRASP signals came from random populations of CA3 neurons. Each eGRASP signal was denoted as a sphere.

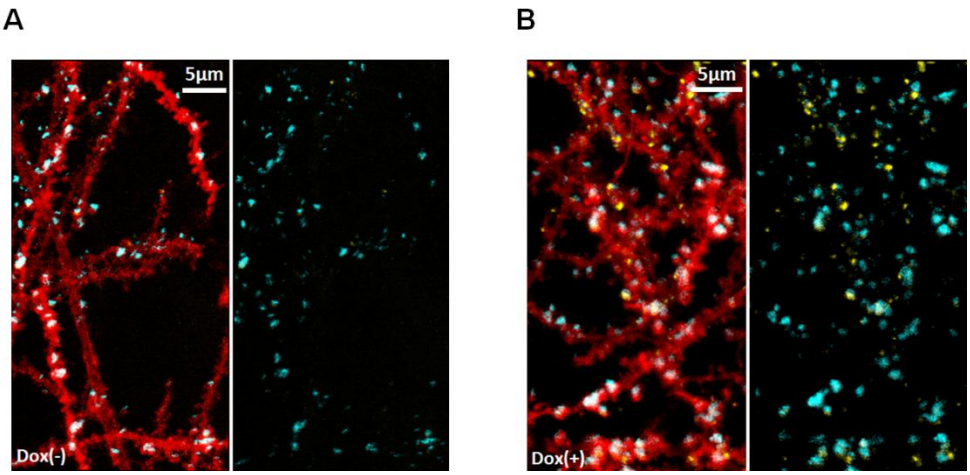

Figure 15. Validation of Yellow eGRASP expression control by doxycycline

(A and B) Representative images of cyan and yellow eGRASP expression without doxycycline (A) or with doxycycline injection (B).

A

	on iRFP670 dendrite
cyan & yellow overlap / cyan	40.25 %
cyan & yellow overlap / yellow	78.38 %

B

	on mScarlet-I dendrite
cyan & yellow overlap / cyan	50.00 %
cyan & yellow overlap / yellow	80.37%

C

iRFP670 & mScarlet-I overlap / iRFP670	20.93 %
iRFP670 & mScarlet-I overlap / mScarlet-I	11.61%

Figure 16. Overlapping percentage of neuronal populations

(A) The percentage of cyan signal that also contains yellow signal on iRFP670 positive dendrites is 40.25 %. The percentage of yellow signal that also contains cyan signal on iRFP670 positive dendrites is 78.38 %. n=43. 43 iRFP670 dendrites from 3 mice.

(B) The percentage of cyan signal that also contains yellow signal on mScarlet-I positive dendrites is 50.00 %. The percentage of yellow signal that also contains cyan signal on mScarlet-I positive dendrites is 80.37 %, n=45, 45 mScarlet-I dendrites from 3 mice.

(C) The percentage of iRFP670 positive cells that also express mScarlet-I is 20.93 %. The percentage of mScarlet-I positive cells that also express iRFP670 is 11.61 %. n=10, 10 CA1 cell layer images from 3 mice.

Increased synaptic density and spine size between CA3 engram and CA1 engram cells by memory formation

Using the 3D modeling, I measured the synaptic density of four types of synapses. I did not found any significant differences between the density of N-N and N-E synapses (Fig. 17A). However, the density of E-E synapses was significantly increased than E-N synapses (Fig. 17B). This increased density of E-E synapses was reproduced regardless of the strength of protein-protein interaction domain in cyan pre-eGRASP, which was constitutively expressed (Fig. 18). These results indicate that the presynaptic terminals coming from CA3 engram cells predominantly synapsed on CA1 engram cells than CA1 non-engram cells after memory formation.

In addition, because it is well demonstrated that spine size is correlated with synaptic potentiation (Hayashi-Takagi et al., 2015; Lamprecht and LeDoux, 2004; Matsuzaki et al., 2004; Tanaka et al., 2008), I further examined spine size. As a result, E-E spine head diameter and spine volume were significantly higher than N-E synaptic spines, while N-N and E-N did not show any significant differences (Fig. 19). Collectively, these results indicate that E-E synapses show higher structural connectivity both in the number of synapses and the size of the spines.

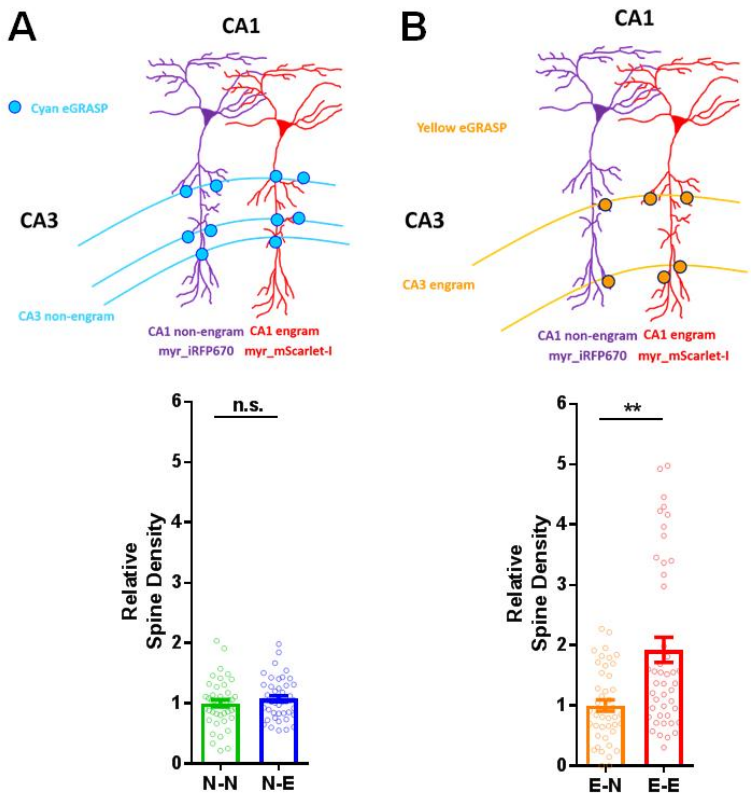

Figure 17. Higher synaptic density of synapses between CA3 engram and CA1 engram cells after memory formation

(A and B) The densities of cyan-only (A) or yellow puncta (B) on mScarlet-I positive dendrites are normalized to the corresponding cyan-only or yellow puncta on iRFP670 positive dendrites from the same images for exclusion of the effect of different number of CA3 cells expressing each presynaptic components. Each data point represents a dendrite. n = 43 for CA1 non-engram dendrites, n = 45 for CA1 engram dendrites, 9 images from 3 mice, Mann Whitney two-tailed test, n.s.: not significant, **p = 0.0017.

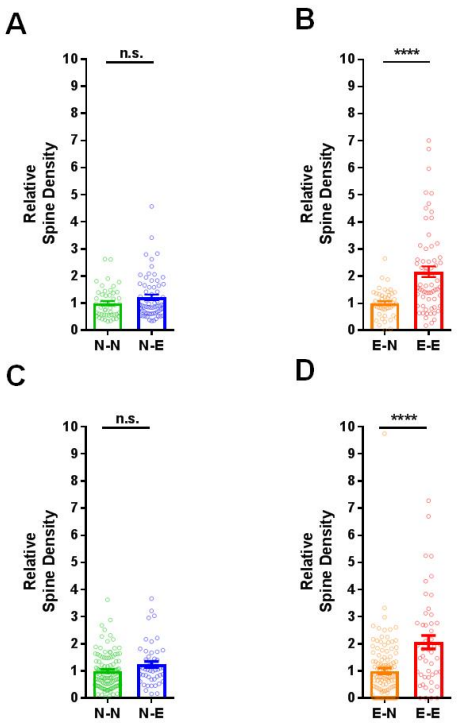

Figure 18. Effect of different interaction strength on synaptic density

(A and B) The experimental design was identical as Figure 17 except that the red fluorescent protein was TagRFP-T instead of mScarlet-I. The results using pre-eGRASP constructs with p32 interacting peptides for both cyan and yellow eGRASP. Synaptic density for N-N synapses is comparable with N-E synapses. However, synaptic density for E-E synapses is significantly higher than E-N synapses. Each data point represents a dendrite. n = 47 for CA1 non-engram dendrites, and n = 64 for CA1 engram dendrites, 11 images from 5 mice, Mann Whitney two-tailed test, n.s.: not significant, ****$p < 0.0001$.

(C and D) The experimental design was identical as Figure 17 except that the red fluorescent protein was TagRFP-T instead of mScarlet-I. The results using pre-eGRASP constructs with p30 interacting peptides for cyan, and p32 interacting

peptides for yellow eGRASP. Synaptic density for N-N synapses is comparable with N-E synapses. However, synaptic density for E-E synapses is significantly higher than E-N synapses. Each data point represents a dendrite. n = 116 for CA1 non-engram dendrites, n = 48 for CA1 engram dendrites, 9 images from 4 mice, Mann Whitney two-tailed test, n.s.: not significant, ****$p < 0.0001$. Data are represented as mean ± SEM.

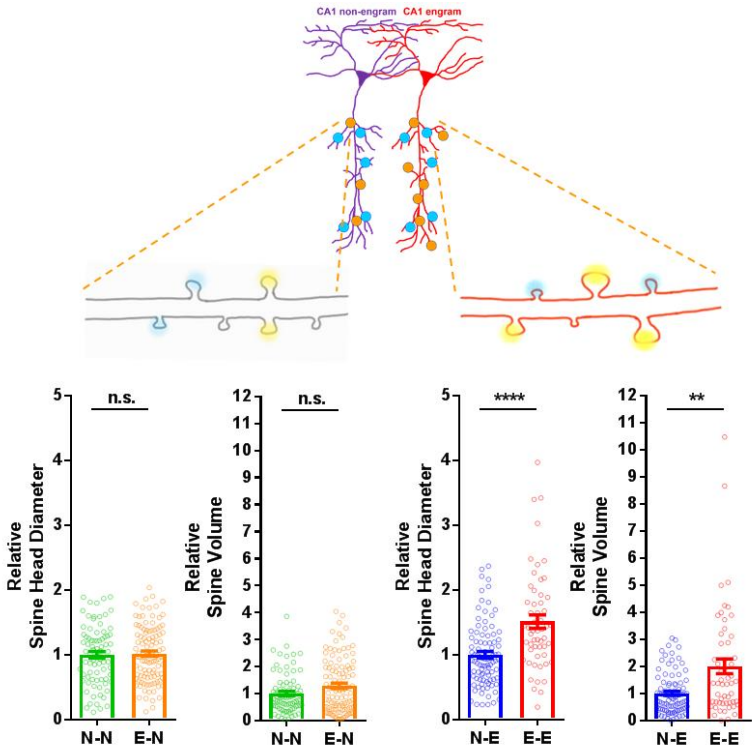

Figure 19. CA3 engram to CA1 engram synapses exhibited larger spine size after memory formation

(Top) Schematic illustration of experiment design and expected results.

(Bottom) Relative spine head diameters and spine volumes of dendrites from CA1 non-engram cells (left) and engram cells (right). Head diameter and volume of the spines with yellow puncta were normalized to those of the spines with cyan-only puncta of the same dendrite. Each data point represents a spine. N-N, n = 81; E-N, n = 107; N-E, n = 93; E-E, n = 55, Mann Whitney two-tailed test, n.s.: not significant, **p = 0.0014, ****p < 0.0001. Data are represented as mean ± SEM.

DISCUSSION

It is widely accepted that the enhancement of synapses between co-activated cells store memory. Despite its importance, previous engram studies remained at the neuron-level because distinguishment of synapses on one dendrite is impossible. Here, I applied the newly developed dual-eGRASP technique, which provides the classification of synapses on single dendrite based on their presynaptic neuronal population in the rodent brain, to find synaptic engram.

First, I validated Fos-rtTA system to capture the activated neurons during learning. Validation using seizure and CFC strongly supported the ability of Fos-rtTA system to capture the neuronal population activated during specific events. To capture the activated neuronal population, previous studies mostly used Fos-tTA transgenic mice. Fos-rtTA system delivered by AAV might have advantages such as ease for mice supplement and adjustment of expression level in various brain regions.

Using Fos-rtTA system and dual-eGRASP, I examined all kinds of connectivity between CA3 and CA1 and found that increased structural connectivity between CA3 engram and CA1 engram cells. Compared with recent studies defined memory engram at neuron-level, I found the memory engram at synapse-level with more sophisticated techniques.

Several studies have found that dendritic spine density and spine morphology are changed following memory formation (Chen et al., 2010; Leuner et al., 2003; Matsuzaki et al., 2001; Matsuzaki et al., 2004). Moreover, a recent study clearly showed that shrinkage of recently potentiated spines induced memory

disruption (Hayashi-Takagi et al., 2015). However, because these studies just observed and manipulated activated spines regardless of its pre and postsynaptic neurons, we still do not know whether synapses between co-activated neurons indeed undergo potentiation to encode memory. Technical limitations, including impossibility to distinguish synapses according to whether their presynaptic neuronal population is engram cells or not, precluded examinations of synapse specific plasticity. In this chapter, I overcame this limitation with dual-eGRASP and found that potentiated synapses, which are known to be responsible for memory encoding by previous studies, are indeed between engram cells. These results strongly support that memory is encoded by Hebbian plasticity, "Fire together, Wire together".

Taken together, these results demonstrate that synapses among engram cells develop experience-dependent structural enhancement to form a memory trace.

CHAPTER IV

Enhanced synaptic transmission between CA3 engram and CA1 engram cells through pre- and post-synaptic mechanisms

INTRODUCTION

In the previous chapter, I found enhanced structural connectivity between CA3 engram to CA1 engram cells. Because the changes in synaptic density and spine morphology are known to be closely related with synaptic transmission efficacy (Bosch and Hayashi, 2012; Engert and Bonhoeffer, 1999; Lamprecht and LeDoux, 2004), these results strongly imply that the synaptic transmission between CA3 engram to CA1 engram cells are specifically increased. Therefore, I examined the changes of synaptic transmission between CA3 to CA1 connections.

Early studies have tried to examine the changes in synaptic connectivity of engram cells. For example, Susumu Tonegawa and his colleagues reported that postsynaptic enhancement of synaptic transmission in DG engram cells (Ryan et al., 2015). However, comparison of the full combinations of connections between engram and non-engram cells in two directly connected regions are needed to elucidate the synaptic mechanism of memory formation.

In this chapter, I investigated the changes of synaptic transmission of four possible combinations of CA3 to CA1 connections after memory formation. To compare presynaptic potentiation according to whether their presynaptic neurons are engram cells or not, I measured paired-pulse ratio (PPR) of four types of connections and found that increased release probability of inputs from CA3 engram cells. Moreover, I found postsynaptic potentiation of CA1 engram cells. Finally, I examined the complete occlusion of pairing LTP between CA3 engram to CA1 engram cells. These results suggest that synapses between engram cells exhibit enhancement of functional connectivity.

EXPERIMENTAL PROCEDURES

Animals

All experiments were performed on 8~10-week-old male C57BL/6N mice purchased from Samtako. Bio. Korea. Mice were raised in 12-hr light/dark cycle in standard laboratory cages and given ad libitum access to food and water. All procedures and animal care followed the regulation and guidelines of the Institutional Animal Care and Use Committees (IACUC) of Seoul National University.

AAV production

Adeno-Associated Viruses serotype 1/2 (AAV1/2; AAV particle that contains both serotype 1 and 2 capsids) were used in all the experiments. AAV1/2s were purified from HEK293T cells that were transfected with plasmids containing each expression cassette flanked by AAV2 ITRs, p5E18, p5E18-RXC1 and pAd-ΔF6 and cultured in 18 ml or 8 ml Opti-MEM (Gibco-BRL/Invitrogen, cat# 31985070) in a 150-mm or 100-mm culture dish, respectively. Four days after transfection, the medium containing AAV1/2 particles was collected and centrifuged at 3,000 rpm for 10 min. After 1 ml of heparin-agarose suspension (Sigma, cat# H6508) was loaded onto a poly-prep chromatography column (Bio-Rad Laboratories, Inc. cat# 731-1550), the supernatant was loaded onto the column carefully. The column was washed by 4 ml of Buffer 4-150 (150 mM NaCl, pH4

10 mM citrate buffer) and 12 ml of Buffer 4-400 (400 mM NaCl, pH4 10 mM citrate buffer). The virus particles were eluted by 4 ml of Buffer 4-1200 (1.2 M NaCl, pH4 10 mM citrate buffer). The eluted solution was exchanged with PBS and concentrated using an Amicon Ultra-15 centrifugal filter unit (Millipore, cat# UFC910024). The titer was measured using quantitative RT-PCR.

Stereotaxic surgery

Mice (8~10 weeks) were anesthetized with a ketamine/xylazine solution and positioned in a stereotaxic apparatus (Stoelting Co.). The virus was injected using 33 gauge needle with Hamilton syringe at a 0.1 μl/min rate into target regions. At all injected points, the tip of the needle was positioned 0.05mm below the target coordinate and returned to the target site after 2min. After injection, the needle stayed in place for an additional 7 mins and was withdrawn slowly. Stereotaxic coordinates for each target sites are left CA3 (double injection: AP: -1.75/ ML: -2.35/ DV: -2.45, AP: -2.25/ ML: -2.7/ DV: -2.65) and right CA1 (AP:-1.8/ ML:+1.5/ DV: -1.65 below the skull surface).

0.5 μl of a mixture of viruses (2.0x107 vg/μl Fos-rtTA3G, 3.37x109 vg/μl of TRE3G-ChrimsonR-mEmerald, 1.0x108 vg/μl of CaMKIIα-Chronos-mCherry) was injected into the left CA3. 0.5 μl of a mixture of viruses (2.0x107 vg/μl Fos-rtTA3G, 1.6x109 vg/μl of TRE3G-mEmerald-Nuc) was injected into right CA1.

Contextual fear conditioning

All mice were conditioned 2~4 weeks after the AAV injection. Each mouse was single caged 10 days before conditioning and was habituated to the hands of the investigator and anesthesia chamber without isoflurane for 3 minutes on each of 7 consecutive days. Mice were conditioned 2 days after the last habituation day. On the conditioning day, 250 μl of 5 mg/ml Doxycycline solution dissolved in saline was injected by intraperitoneal injection during brief anesthesia by isoflurane in the anesthesia chamber 2 hours prior to the conditioning. Conditioning sessions were 300s in duration, and three 0.6 mA shocks of 2 s duration were delivered at 208 s, 238 s, and 268 s from the initiation of the session in a square chamber with a steel grid (Med Associates Inc., St Albans, VT). When the conditioning was finished, mice were immediately transferred to their homecage. 2 days after the conditioning, mice were carefully decapitated for recording experiments.

Electrophysiology

To improve slice conditions in adult hippocampal slices, we used N-methyl-D-glucamine (NMDG) solution (93 mM NMDG, 2.5 mM KCl, 1.2 mM NaH2PO4, 30mM NaHCO3, 20mM HEPES, 25mM Glucose, 5mM sodium ascorbate, 2mM Thiourea, 3mM sodium pyruvate, 10mM MgSO4, 0.5mM CaCl2) for brain slicing and recovery 32. Mice were deeply anesthetized by intraperitoneal injection of Ketamine/Xylazine mixture and then transcardially perfused with ice-cold NMDG solution. Following cardiac perfusion, the coronal slices (300~400-

μm thick) were prepared using a vibratome (VT1200S; Leica) in ice-cold NMDG solution, and then recovered in NMDG solution at 32-34 ℃ for 10 min.

After recovery, the slices were transferred to modified HEPES holding ACSF (92 mM NaCl, 2.5 mM KCl, 1.2 mM NaH2PO4, 30 mM NaHCO3, 20 mM HEPES, 25 mM Glucose, 5 mM sodium ascorbate, 2 mM Thiourea, 3 mM sodium pyruvate, 2 mM MgSO4, 2 mM CaCl2) at room temperature (RT) and allowed to recover for at least 1h. After recovery, the slice was transferred to the recording chamber constantly perfused with RT standard ACSF (124 mM NaCl, 2.5 mM KCl, 1 mM NaH2PO4, 25 mM NaHCO3, 10 mM glucose, 2 mM CaCl2, and 2 mM MgSO4). The recording pipettes (3~5 MΩ) were filled with an internal solution containing (in mM) 145 K-gluconate, 5 NaCl, 10 HEPES, 1 MgCl2, 0.2 EGTA, 2 MgATP, and 0.1 Na3GTP (280~300 mOsm, adjust to pH 7.2 with KOH). Picrotoxin (100 μM) was added to the ACSF to block the GABA-R-mediated currents.

Blue light was delivered by 473 nm DPSS laser (Laserglow Technologies Inc.) and yellow light was delivered by 593 nm DPSS laser (OEM Laser Systems). Light intensity was adjusted to elicit a reliable synaptic response 33. For Sr^{2+} light-evoked mEPSC experiments, we used modified ACSF containing 4 mM MgCl2 and 4 mM SrCl2 instead of CaCl2. Light was delivered for a duration of 300 ms. To exclude the synchronous release component, mEPSC events in 60 – 400 ms post light stimulation were analyzed by MiniAnalysis program (Synaptosoft). For pairing-LTP experiments, EPSCs were evoked at 0.05 Hz and three successive EPSCs were averaged and expressed relative to the normalized baseline. To induce

pairing-LTP, four brief high-frequency tetani (50 pulses of 20 Hz per each; 4 s intervals) paired with a long depolarization (3 min to 0 mV) given at the end of the long depolarization. Hippocampal neurons were voltage-clamped at -70 mV using an Axopatch 200B (Molecular Devices). Only cells with a change in access resistance <20% were included in the analysis. mEmerald-nuc expression was confirmed by a cooled CCD camera (ProgRes MF cool; Jenoptik) and fluorescence microscope (BX51WI; Olympus).

Electrophysiology

Data were analyzed using Prism software. Tukey's multiple comparison test after one-way ANOVA was used to test for statistical significance when appropriate. The exact value of n and statistical significance are reported in the figure legends.

RESULTS (Collaborated with Dr. Su-Eon Sim)

Strategy for electrophysiological recordings

To achieve the specific recording of four types of synapses according to its pre- and postsynaptic neurons, I selectively stimulated inputs from CA3 engram cells using ChrimsonR, while the total population of CA3 neurons using Chronos. These opsins can be independently activated by lasers with different wavelengths, specifically blue and yellow lasers, respectively (Klapoetke et al., 2014). I expressed ChrimsonR in CA3 engram cells using Fos-rtTA system, while Chronos was expressed primarily in CA3 excitatory cells under the CaMKIIα promoter (Choi et al., 2014). Then, CA3 engram cells and total population could be selectively activated by different lasers. In addition, through labeling CA1 engram cells with nucleus-targeted mEmerald (mEmerald-Nuc) using Fos-rtTA (Fig. 20A), selective whole-cell patch recordings from either CA1 engram or non-engram cells were possible. Optical stimulation with 473 nm blue light or 593 nm yellow light produced reliable EPSCs on both CA1 engram and non-engram cells. Using this system, I investigated the four kinds of synaptic responses in a single hippocampal slice: total excitatory to non-engram (T-N), total excitatory to engram (T-E), engram to non-engram (E-N) and engram to engram (E-E) (Fig. 20B).

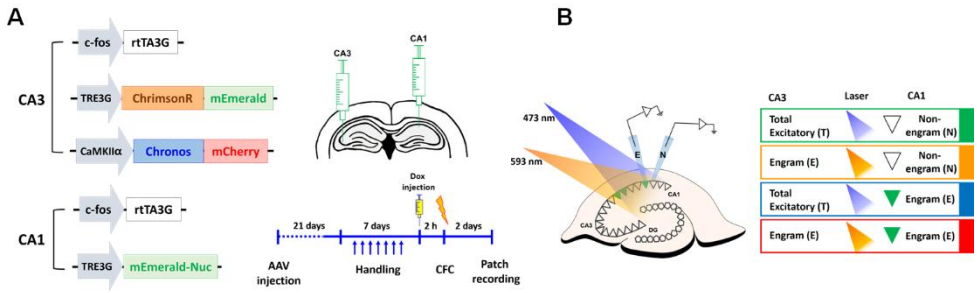

Figure 20. Schematic illustration of electrophysiological experiments

(A) (Left) Schematics of injected AAVs. (Right) illustration of virus injection sites and experimental protocol.

(B) (Left) Diagram showing whole-cell patch recording. (Right) Classification of the four synaptic populations indicated by four colors. Green, T-N; Orange, E-N; Blue, T-E; Red, E-E. The colors for each group are applied to Chapter IV.

Both pre- and post-synaptic mechanisms are the basis for enhanced synaptic transmission between CA3 engram and Ca1 engram cells.

First, I investigated presynaptic potentiation through PPR which is one of the indicators of release probability and presynaptic potentiation. As a result, PPR of inputs from CA3 engram was significantly decreased at 25-, 50-, and 75-ms interstimulus intervals than it from non-engram. These results imply increased release probability from CA3 engram inputs to CA1. The decrease was most prominent in E-E synaptic responses (Fig. 21).

I then examined postsynaptic α-amino-3-hydroxy-5-methyl-4-isoxazolepropionic acid (AMPA) receptor levels in synapses from the four combinations of synaptic responses by replacing Ca^{2+} with Sr^{2+} in the external recording solution. Sr^{2+} can substitute for Ca^{2+} and trigger neurotransmitter release, but its clearance and buffering are less effective than Ca^{2+} (Dodge et al., 1969; Xu-Friedman and Regehr, 1999). Because Sr^{2+} desynchronized evoked synaptic release, and induced prolonged asynchronous release, which enabled examination of quantal synaptic responses (Fig. 22A), I could measure the amplitude of evoked miniature EPSCs (mEPSCs) 60 - 400 ms after light delivery. The levels of postsynaptic AMPA receptors of synapses on CA1 engram cells were significantly increased compared to that on CA1 non-engram cell (Fig. 22B), which indicated that after memory formation, the synapses of CA1 engram cells were potentiated while synapses of CA1 non-engram cells were not.

Changes in both presynaptic release probability and postsynaptic potentiation are known to be crucial for long-term potentiation (LTP) (Bliss and Collingridge, 2013). Therefore, to test whether LTP is induced during memory formation, the extents of LTP occlusion were examined by inducing pairing LTP separately in the four synaptic types (Chen et al., 1999). Pairing LTP stimuli were delivered after 5 min of baseline recording. I found robustly enhanced T-N synaptic responses (~150%). T-E and E-N synaptic responses were also potentiated. The potentiation levels were lower than T-N synaptic responses (~120%), but these differences were not significant. Interestingly, I also found that pairing LTP in E-E synaptic responses was completely blocked and potentiation level was significantly lower than T-N synaptic responses (Fig. 23). These results suggest that the combined effect of increased probability of presynaptic release from CA3 engram cells and potentiation of postsynaptic responses on CA1 engram cells induces specific and strong LTP at engram to engram synapses.

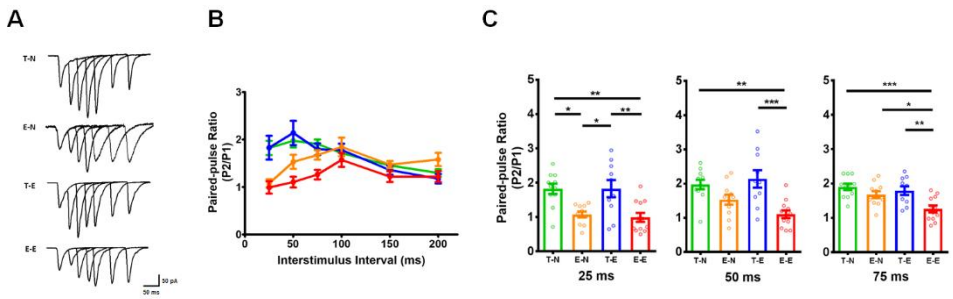

Figure 21. Presynaptic enhancement of synapses receive input from CA3 engram cells

(in collaboration with Dr. Su-Eon Sim)

(A) Represent traces from PPR recordings.

(B) Results of PPR recordings. T-N, n = 11; T-E, n = 10; E-N, n = 11; E-E, n = 12.

(C) Average PPR at the indicated interstimulus intervals. *p < 0.05, **p < 0.01, ***p < 0.001, Tukey's multiple comparison test after one-way ANOVA; (25 ms) F(3,40) = 8.259, *p = 0.0276; (50 ms) F(3,40) = 7.989, ***p = 0.0003; (75 ms) F(3,40) = 7.517, ***p = 0.0004. Data are represented as mean ± SEM.

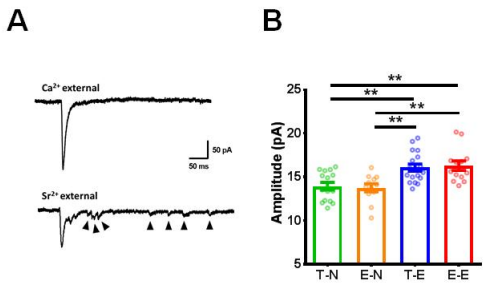

Figure 22. Postsynaptic enhancement of synapses on dendrite from CA1 engram cells

(in collaboration with Dr. Su-Eon Sim)

(A) Traces of light-evoked mEPSCs using Ca^{2+} or Sr^{2+} external solutions. Arrowheads indicate quantal release events.

(B) Average amplitude of the Sr^{2+} light-evoked mEPSCs of each synaptic transmissions. T-N, n = 15; T-E, n = 18; E-N, n = 12; E-E, n = 13; **p < 0.01, Tukey's multiple comparison test after one-way ANOVA, $F(3,54) = 8.540$, ***p < 0.0001. Data are represented as mean ± SEM.

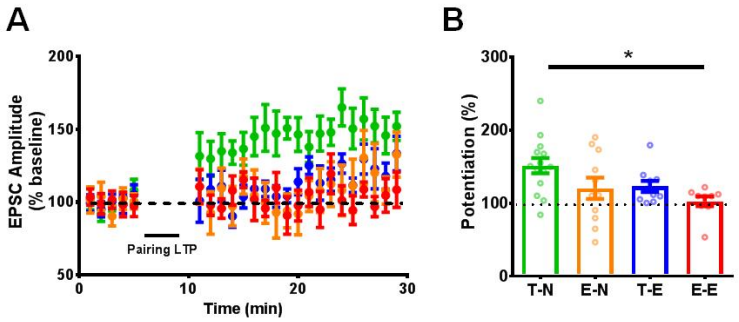

Figure 23. LTP occlusion of pairing LTP in each of the four synaptic types in CA1

(in collaboration with Dr. Su-Eon Sim)

(A) Changes of ESPC amplitude after pairing LTP stimulus with 5 min of baseline recording. T-N, n = 14; T-E, n = 10; E-N, n = 11; E-E, n = 9.

(B) Average relative potentiated levels of EPSC amplitude in the last 5 min of recording. *p < 0.05, Tukey's multiple comparison test after one-way ANOVA, $F(3,40) = 3.683$, *p = 0.0197. Data are represented as mean ± SEM.

DISCUSSION

In this chapter, I found the functional enhancement of synaptic transmission, which was induced by the synergistic effect of pre- and postsynaptic mechanism, between CA3 engram and CA1 engram cells using electrophysiological experiments. These results are strongly supported by the enhancement of structural connectivity between engram cells which was found in Chapter III.

Using Chronos and ChrimsonR expressed by different promoters, I successfully compared presynaptic properties in one neuron according to its presynaptic neuronal population. Because many brain regions are received inputs from more than two presynaptic regions, this approach might be applicable in various brain regions for direct comparison of the properties and functions of input from different presynaptic neuronal population to one neuron.

The findings of this study might provide us with clue for elucidating the mechanism of LTP, particularly between CA3 and CA1. A contested debate remains whether the mechanism of LTP between CA3 and CA1 comprises presynaptic or postsynaptic potentiation (Bliss and Collingridge, 1993). Some reports support that the presynaptic mechanisms, including an increase in the probability of neurotransmitter release, is crucial for LTP (Lauri et al., 2007). However, some reports strongly support that the postsynaptic rather than presynaptic mechanisms, such as the increased efficacy of postsynaptic receptors, are the genuine mechanism for LTP (Kerchner and Nicoll, 2008; Wu and Saggau, 1994).

Decreased PPR implies the presynaptic potentiation of synapses innervated from CA3 engram cells. In addition, enhanced amplitude of mEPSC implies the postsynaptic potentiation of synapses on dendrites of CA1 engram cells. Therefore, results in this chapter implicate that both presynaptic and postsynaptic mechanisms work synergistically to potentiate synapses for LTP and encoding memory.

The most potentiated E-E connections, which showed the complete occlusion of LTP and the most extent of changes of PPR and mEPSC amplitude, supported the Hebbian plasticity. However, interestingly, PPR of E-N connections is more decreased than that of T-N connections. In addition, mEPSC amplitude of N-E connections is more increased than that of N-N connections. These results imply that if only one side of pre- or postsynaptic neurons is engram cell, the functional potentiation process might partially occur. These results might support the other potentiation mechanism rather than Hebbian plasticity that emphasize both pre- and postsynaptic mechanisms. It might be an interesting study to elucidate how these different potentiation mechanisms synergistically collaborate to encode memory.

CHAPTER V

CONCLUSION

CONCLUSION

In this study, I developed dual-eGRASP, which is a novel dual-color synapse-labeling technique, and investigated that synapses between engram cells are specifically enhanced after memory formation in structural and functional aspects by imaging and recording experiments.

In Chapter II, I focused on the development of dual-eGRASP technique to achieve distinguishment of synapses on one dendrite according to their presynaptic neuronal populations. I enhanced the fluorescent signal of split GFP by introducing a widely used mutation and weak interaction domains to enhance the reconstitution of split GFP. In addition, distinguishable dual-color (cyan and yellow) split FP were produced by rationally selected mutations. I confirmed that the cyan and yellow fluorescent signals were clearly separated on the membrane of HEK293T cells. Finally, I applied dual-eGRASP into mouse brain regions such as DG and CA1, then successfully distinguished synapses based on their presynaptic regions.

In Chapter III, I compared all possible combinations of synapses (N-N, N-E, E-N, E-E) between CA3 to CA1 connections using dual-eGRASP combined with Fos-rtTA system, which allows expression of genes of interest in activated neurons during specific events. I discovered that synaptic density and spine morphology of synapses between CA3 engram to CA1 engram cells are specifically enlarged after memory formation.

In Chapter IV, I found the enhanced synaptic transmission between engram cells by electrophysiological experiments using Chronos and ChrimsonR. I observed a decreased PPR of input from CA3 engram cells. This result implies the

increase of presynaptic release probability of presynaptic engram cells. In addition, I found increased mEPSC amplitudes of synapses on CA1 engram cells which mean the postsynaptic potentiation of postsynaptic engram cells. I also found the complete occlusion of pairing LTP of E-E connections which may occur by synergistic effects of increased presynaptic release probability and postsynaptic potentiation. These results strongly support the enhancement of functional connectivity between engram cells at synapse-level.

Many studies have focused on the finding of memory engram. To my knowledge, this is the first study to reveal the specific enhancement of synapses between engram cells by comparison of the full combination of connections among engram and non-engram cells in two directly connected regions. There are remaining issues to be elucidated in future studies. This study showed the correlation of the synaptic potentiation between engram cells and memory formation, but not the causality. If the causality is proved using a specific manipulation of synapses between engram cells, it might be strong evidence supporting the idea that synaptic engram indeed encodes the specific memory. In addition, recent studies have demonstrated that the place encoding memory might be dynamically changed in inter- and intraregional level (Davis and Reijmers, 2017; Frankland and Bontempi, 2005; Hainmueller and Bartos, 2018; Mankin et al., 2012; Rubin et al., 2015). Therefore, future studies should reveal how long lasting the enhancement of synapses between engram cells and more importantly, how our brain keep the qualitatively same memory, despite the memory engrams are dynamic.

Collectively, this study clearly revealed that Hebbian plasticity indeed

occurs during memory encoding process in CA3 to CA1 synapses. This innovative approach might support the idea that synapses among engram cells are the engram synapses that encode memory, not the engram cells themselves.

REFERENCES

Amaral, D.G., Scharfman, H.E., and Lavenex, P. (2007). The dentate gyrus: fundamental neuroanatomical organization (dentate gyrus for dummies). Prog Brain Res *163*, 3-22.

Bindels, D.S., Haarbosch, L., van Weeren, L., Postma, M., Wiese, K.E., Mastop, M., Aumonier, S., Gotthard, G., Royant, A., Hink, M.A., *et al.* (2017). mScarlet: a bright monomeric red fluorescent protein for cellular imaging. Nature Methods *14*, 53-56.

Blair, H.T., Schafe, G.E., Bauer, E.P., Rodrigues, S.M., and LeDoux, J.E. (2001). Synaptic plasticity in the lateral amygdala: a cellular hypothesis of fear conditioning. Learning & memory *8*, 229-242.

Bliss, T.V., and Collingridge, G.L. (1993). A synaptic model of memory: long-term potentiation in the hippocampus. Nature *361*, 31-39.

Bliss, T.V., Collingridge, G.L., Kaang, B.-K., and Zhuo, M. (2016). Synaptic plasticity in the anterior cingulate cortex in acute and chronic pain. Nature Reviews Neuroscience *17*, 485.

Bliss, T.V., and Lømo, T. (1973). Long-lasting potentiation of synaptic transmission in the dentate area of the anaesthetized rabbit following stimulation of the perforant path. The Journal of physiology *232*, 331-356.

Bliss, T.V.P., and Collingridge, G.L. (2013). Expression of NMDA receptor-dependent LTP in the hippocampus: bridging the divide. Molecular Brain *6*, 5.

Bosch, M., and Hayashi, Y. (2012). Structural plasticity of dendritic spines. Current

opinion in neurobiology *22*, 383-388.

Briggman, K.L., and Bock, D.D. (2012). Volume electron microscopy for neuronal circuit reconstruction. Current opinion in neurobiology *22*, 154-161.

Chen, H.-X., Otmakhov, N., and Lisman, J. (1999). Requirements for LTP induction by pairing in hippocampal CA1 pyramidal cells. Journal of Neurophysiology *82*, 526-532.

Chen, Y., Rex, C.S., Rice, C.J., Dube, C.M., Gall, C.M., Lynch, G., and Baram, T.Z. (2010). Correlated memory defects and hippocampal dendritic spine loss after acute stress involve corticotropin-releasing hormone signaling. Proceedings of the National Academy of Sciences of the United States of America *107*, 13123-13128.

Choi, J.-H., Yu, N.-K., Baek, G.-C., Bakes, J., Seo, D., Nam, H.J., Baek, S.H., Lim, C.-S., Lee, Y.-S., and Kaang, B.-K. (2014). Optimization of AAV expression cassettes to improve packaging capacity and transgene expression in neurons. Molecular Brain *7*, 17.

Cowansage, K.K., Shuman, T., Dillingham, B.C., Chang, A., Golshani, P., and Mayford, M. (2014). Direct Reactivation of a Coherent Neocortical Memory of Context. Neuron *84*, 432-441.

Davis, P., and Reijmers, L.G. (2017). The dynamic nature of fear engrams in the basolateral amygdala. Brain research bulletin.

De Robertis, E.D., and Bennett, H.S. (1955). Some features of the submicroscopic morphology of synapses in frog and earthworm. The Journal of Cell Biology *1*, 47-58.

Denny, C.A., Kheirbek, M.A., Alba, E.L., Tanaka, K.F., Brachman, R.A., Laughman, K.B., Tomm, N.K., Turi, G.F., Losonczy, A., and Hen, R. (2014).

Hippocampal Memory Traces Are Differentially Modulated by Experience, Time, and Adult Neurogenesis. Neuron *83*, 189-201.

Dodge, F.A., Miledi, R., and Rahamimoff, R. (1969). Strontium and quantal release of transmitter at the neuromuscular junction. The Journal of Physiology *200*, 267-283.

Druckmann, S., Feng, L., Lee, B., Yook, C., Zhao, T., Magee, J.C., and Kim, J. (2014). Structured synaptic connectivity between hippocampal regions. Neuron *81*, 629-640.

Engert, F., and Bonhoeffer, T. (1999). Dendritic spine changes associated with hippocampal long-term synaptic plasticity. Nature *399*, 66.

Finnerty, G.T., and Jefferys, J.G. (1993). Functional connectivity from CA3 to the ipsilateral and contralateral CA1 in the rat dorsal hippocampus. Neuroscience *56*, 101-108.

Frankland, P.W., and Bontempi, B. (2005). The organization of recent and remote memories. Nature reviews Neuroscience *6*, 119-130.

Fredj, A., Pasquier, H., Demachy, I., Jonasson, G., Levy, B., Derrien, V., Bousmah, Y., Manoussaris, G., Wien, F., and Ridard, J. (2012). The single T65S mutation generates brighter cyan fluorescent proteins with increased photostability and pH insensitivity. PLoS One *7*, e49149.

Goedhart, J., Von Stetten, D., Noirclerc-Savoye, M., Lelimousin, M., Joosen, L., Hink, M.A., Van Weeren, L., Gadella Jr, T.W., and Royant, A. (2012). Structure-guided evolution of cyan fluorescent proteins towards a quantum yield of 93%. Nature communications *3*, 751.

Haasteren, G.v., Li, S., Ryser, S., and Schlegel, W. (2000). Essential Contribution

of Intron Sequences to Ca2+-Dependent Activation of c-fos Transcription in Pituitary Cells. NEN *72*, 368-378.

Hainmueller, T., and Bartos, M. (2018). Parallel emergence of stable and dynamic memory engrams in the hippocampus. Nature *558*, 292-296.

Han, J.-H., Kushner, S.A., Yiu, A.P., Hsiang, H.-L.L., Buch, T., Waisman, A., Bontempi, B., Neve, R.L., Frankland, P.W., and Josselyn, S.A. (2009). Selective erasure of a fear memory. Science *323*, 1492-1496.

Han, J.H., Kushner, S.A., Yiu, A.P., Cole, C.J., Matynia, A., Brown, R.A., Neve, R.L., Guzowski, J.F., Silva, A.J., and Josselyn, S.A. (2007). Neuronal competition and selection during memory formation. Science *316*, 457-460.

Hayashi-Takagi, A., Yagishita, S., Nakamura, M., Shirai, F., Wu, Y.I., Loshbaugh, A.L., Kuhlman, B., Hahn, K.M., and Kasai, H. (2015). Labelling and optical erasure of synaptic memory traces in the motor cortex. Nature *525*, 333-338.

Hebb, D.O. (1949). The organization of behavior: A neuropsychological theory (New York, NY: Wiley).

Helmstaedter, M. (2013). Cellular-resolution connectomics: challenges of dense neural circuit reconstruction. Nature methods *10*, 501.

Huber, K.M., Gallagher, S.M., Warren, S.T., and Bear, M.F. (2002). Altered synaptic plasticity in a mouse model of fragile X mental retardation. Proceedings of the National Academy of Sciences *99*, 7746-7750.

Kerchner, G.A., and Nicoll, R.A. (2008). Silent synapses and the emergence of a postsynaptic mechanism for LTP. Nature reviews Neuroscience *9*, 813-825.

Kim, J., Kwon, J.T., Kim, H.S., Josselyn, S.A., and Han, J.H. (2014). Memory recall and modifications by activating neurons with elevated CREB. Nat Neurosci

17, 65-72.

Kim, J., Zhao, T., Petralia, R.S., Yu, Y., Peng, H., Myers, E., and Magee, J.C. (2011). mGRASP enables mapping mammalian synaptic connectivity with light microscopy. Nat Methods *9*, 96-102.

Kim, J.I., Cho, H.Y., Han, J.H., and Kaang, B.K. (2016). Which Neurons Will Be the Engram - Activated Neurons and/or More Excitable Neurons? Exp Neurobiol *25*, 55-63.

Klapoetke, N.C., Murata, Y., Kim, S.S., Pulver, S.R., Birdsey-Benson, A., Cho, Y.K., Morimoto, T.K., Chuong, A.S., Carpenter, E.J., Tian, *Z., et al.* (2014). Independent optical excitation of distinct neural populations. Nature Methods *11*, 338-346.

Köker, T., Fernandez, A., and Pinaud, F. (2018). Characterization of Split Fluorescent Protein Variants and Quantitative Analyses of Their Self-Assembly Process. Scientific reports *8*, 5344.

Lamprecht, R., and LeDoux, J. (2004). Structural plasticity and memory. Nature reviews Neuroscience *5*, 45-54.

Lauri, S.E., Palmer, M., Segerstrale, M., Vesikansa, A., Taira, T., and Collingridge, G.L. (2007). Presynaptic mechanisms involved in the expression of STP and LTP at CA1 synapses in the hippocampus. Neuropharmacology *52*, 1-11.

Lee, H., Oh, W.C., Seong, J., and Kim, J. (2016). Advanced Fluorescence Protein-Based Synapse-Detectors. Front Synaptic Neurosci *8*, 16.

Leuner, B., Falduto, J., and Shors, T.J. (2003). Associative memory formation increases the observation of dendritic spines in the hippocampus. Journal of Neuroscience *23*, 659-665.

Liu, X., Ramirez, S., Pang, P.T., Puryear, C.B., Govindarajan, A., Deisseroth, K., and Tonegawa, S. (2012). Optogenetic stimulation of a hippocampal engram activates fear memory recall. Nature *484*, 381-385.

Loew, R., Heinz, N., Hampf, M., Bujard, H., and Gossen, M. (2010). Improved Tet-responsive promoters with minimized background expression. BMC Biotechnol *10*, 81.

Malenka, R.C. (1994). Synaptic plasticity in the hippocampus: LTP and LTD. Cell *78*, 535-538.

Mankin, E.A., Sparks, F.T., Slayyeh, B., Sutherland, R.J., Leutgeb, S., and Leutgeb, J.K. (2012). Neuronal code for extended time in the hippocampus. Proceedings of the National Academy of Sciences *109*, 19462-19467.

Martin, S.J., Grimwood, P.D., and Morris, R.G. (2000). Synaptic plasticity and memory: an evaluation of the hypothesis. Annual review of neuroscience *23*, 649-711.

Matsuzaki, M., Ellis-Davies, G.C., Nemoto, T., Miyashita, Y., Iino, M., and Kasai, H. (2001). Dendritic spine geometry is critical for AMPA receptor expression in hippocampal CA1 pyramidal neurons. Nat Neurosci *4*, 1086-1092.

Matsuzaki, M., Honkura, N., Ellis-Davies, G.C., and Kasai, H. (2004). Structural basis of long-term potentiation in single dendritic spines. Nature *429*, 761-766.

Morgan, J.L., and Lichtman, J.W. (2013). Why not connectomics? Nature methods *10*, 494.

Ohkawa, N., Saitoh, Y., Suzuki, A., Tsujimura, S., Murayama, E., Kosugi, S., Nishizono, H., Matsuo, M., Takahashi, Y., Nagase, M.*, et al.* (2015). Artificial Association of Pre-stored Information to Generate a Qualitatively New Memory.

Cell reports.

Palay, S.L., and Palade, G.E. (1955). The fine structure of neurons. The Journal of biophysical and biochemical cytology *1*, 69.

Pisabarro, M.T., and Serrano, L. (1996). Rational Design of Specific High-Affinity Peptide Ligands for the Abl-SH3 Domain. Biochemistry *35*, 10634-10640.

Ramirez, S., Liu, X., Lin, P.A., Suh, J., Pignatelli, M., Redondo, R.L., Ryan, T.J., and Tonegawa, S. (2013). Creating a false memory in the hippocampus. Science *341*, 387-391.

Ramirez, S., Liu, X., MacDonald, C.J., Moffa, A., Zhou, J., Redondo, R.L., and Tonegawa, S. (2015). Activating positive memory engrams suppresses depression-like behaviour. Nature *522*, 335-339.

Reijmers, L.G., Perkins, B.L., Matsuo, N., and Mayford, M. (2007). Localization of a stable neural correlate of associative memory. Science *317*, 1230-1233.

Rubin, A., Geva, N., Sheintuch, L., and Ziv, Y. (2015). Hippocampal ensemble dynamics timestamp events in long-term memory. Elife *4*.

Russo, S.J., Dietz, D.M., Dumitriu, D., Morrison, J.H., Malenka, R.C., and Nestler, E.J. (2010). The addicted synapse: mechanisms of synaptic and structural plasticity in nucleus accumbens. Trends in neurosciences *33*, 267-276.

Ryan, T.J., Roy, D.S., Pignatelli, M., Arons, A.L., and Tonegawa, S. (2015). Engram cells retain memory under retrograde amnesia. Science.

Sano, Y., Shobe, J.L., Zhou, M., Huang, S., Shuman, T., Cai, D.J., Golshani, P., Kamata, M., and Silva, A.J. (2014). CREB Regulates Memory Allocation in the Insular Cortex. Current biology : CB *24*, 2833-2837.

Sawano, A., and Miyawaki, A. (2000). Directed evolution of green fluorescent

protein by a new versatile PCR strategy for site-directed and semi-random mutagenesis. Nucleic acids research *28*, e78-e78.

Selkoe, D.J. (2002). Alzheimer's disease is a synaptic failure. Science *298*, 789-791.

Semon, R. (1921). The mneme (London, UK: G. Allen & Unwin).

Semon, R. (1923). Mnemic psychology (London, UK: G. Allen & Unwin).

Shcherbakova, D.M., and Verkhusha, V.V. (2013). Near-infrared fluorescent proteins for multicolor in vivo imaging. Nat Methods *10*, 751-754.

Shekhawat, S.S., and Ghosh, I. (2011). Split-protein systems: beyond binary protein-protein interactions. Curr Opin Chem Biol *15*, 789-797.

Stephan, K.E., Friston, K.J., and Frith, C.D. (2009). Dysconnection in schizophrenia: from abnormal synaptic plasticity to failures of self-monitoring. Schizophrenia bulletin *35*, 509-527.

Tanaka, J.-i., Horiike, Y., Matsuzaki, M., Miyazaki, T., Ellis-Davies, G.C., and Kasai, H. (2008). Protein synthesis and neurotrophin-dependent structural plasticity of single dendritic spines. Science *319*, 1683-1687.

Tanaka, K.Z., Pevzner, A., Hamidi, A.B., Nakazawa, Y., Graham, J., and Wiltgen, B.J. (2014). Cortical Representations Are Reinstated by the Hippocampus during Memory Retrieval. Neuron *84*, 347-354.

Tayler, K.K., Tanaka, K.Z., Reijmers, L.G., and Wiltgen, B.J. (2013). Reactivation of neural ensembles during the retrieval of recent and remote memory. Current biology : CB *23*, 99-106.

Tonegawa, S., Liu, X., Ramirez, S., and Redondo, R. (2015). Memory Engram Cells Have Come of Age. Neuron *87*, 918-931.

Tsetsenis, T., Boucard, A.A., Araç, D., Brunger, A.T., and Südhof, T.C. (2014).

Direct Visualization of Trans-Synaptic Neurexin–Neuroligin Interactions during Synapse Formation. Journal of Neuroscience *34*, 15083-15096.

Wolf, M.E. (2016). Synaptic mechanisms underlying persistent cocaine craving. Nature Reviews Neuroscience *17*, 351.

Wu, L., and Saggau, P. (1994). Presynaptic calcium is increased during normal synaptic transmission and paired-pulse facilitation, but not in long-term potentiation in area CA1 of hippocampus. Journal of Neuroscience *14*, 645-654.

Xu-Friedman, M.A., and Regehr, W.G. (1999). Presynaptic strontium dynamics and synaptic transmission. Biophysical Journal *76*, 2029-2042.

Yiu, A.P., Mercaldo, V., Yan, C., Richards, B., Rashid, A.J., Hsiang, H.L., Pressey, J., Mahadevan, V., Tran, M.M., Kushner, S.A.*, et al.* (2014). Neurons Are Recruited to a Memory Trace Based on Relative Neuronal Excitability Immediately before Training. Neuron *83*, 722-735.

Zhou, X., Vink, M., Klaver, B., Berkhout, B., and Das, A.T. (2006). Optimization of the Tet-On system for regulated gene expression through viral evolution. Gene Ther *13*, 1382-1390.

Zhou, Y., Won, J., Karlsson, M.G., Zhou, M., Rogerson, T., Balaji, J., Neve, R., Poirazi, P., and Silva, A.J. (2009). CREB regulates excitability and the allocation of memory to subsets of neurons in the amygdala. Nat Neurosci *12*, 1438-1443.

국문초록

기억이 저장되는 원리와 장소를 찾기 위하여 오랜 기간 동안 많은 노력들이 이어져왔다. 최근 연구들에 의하면 기억은 엔그램 세포들에 의해 저장된다는 것이 밝혀졌다. 하지만 기억저장에 있어서 시냅스 가소성의 중요성을 고려했을 때 기억이 저장되는 장소를 세포수준이 아닌 시냅스 수준에서 밝히는 연구가 필요하다. 기술적 한계로 인하여 한 신경세포의 시냅스들을 분류하는 것이 불가능하였기 때문에 어떤 시냅스들이 특이적으로 기억형성에 의해 강화되는지 확인할 수 없었다. 본 연구는 엔그램 세포 사이의 시냅스가 특이적으로 강화되는 것을 보임으로서 엔그램을 시냅스 수준에서 찾아내고자 하였다. 이를 위해 한 수상돌기의 시냅스들을 시냅스 전 신경세포의 종류에 따라 구분해낼 수 있는 dual-eGRASP라는 기술을 개발하였다. 이를 이용하여 CA3 – CA1 사이의 가능한 네 종류의 시냅스 (엔그램 – 엔그램, 엔그램 – 비엔그램, 비엔그램 – 엔그램, 비엔그램 – 비엔그램)들 중에서 엔그램 – 엔그램 시냅스가 개수와 크기 측면에서 특이적으로 증가해있다는 것을 발견하였다. 이에 더하여 전기생리학적 실험으로 CA3 엔그램 시냅스의 분비확률증가와 CA1 엔그램 시냅스의 시냅스 후 반응 증가를 보임으로서 엔그램 세포 사이의 시냅스의 기능적 증가를 증명하였다. 이러한 결과들을 바탕으로 엔그램 세포 사이 시냅스가 구조적, 기능적 증가를 통해 기억을 저장하는 시냅스가 된다고 밝혀내었다.

주요어 : 기억, 해마, 엔그램, 시냅스 가소성

학번 : 2014-21265